LANGMUIR

pubs.acs.org/Langmuir Article

Perspectives on Theoretical Models and Molecular Simulations of Polymer Brushes

Published as part of Langmuir virtual special issue "Highlights in Interface Science and Engineering: Polymer Brushes".

Yijing Tang, Yonglan Liu, Dong Zhang, and Jie Zheng*

Cite This: *Langmuir* 2024, 40, 1487–1502 Read Online

ACCESS | Metrics & More | Article Recommendations

ABSTRACT: Polymer brushes have witnessed extensive utilization and progress, driven by their distinct attributes in surface modification, tethered group functionality, and tailored interactions at the nanoscale, enabling them for various scientific and industrial applications of coatings, sensors, switchable/responsive materials, nanolithography, and lab-on-a-chips. Despite the wealth of experimental investigations into polymer brushes, this review primarily focuses on computational studies of antifouling polymer brushes with a strong emphasis on achieving a molecular-level understanding and structurally designing antifouling polymer brushes. Computational exploration covers three realms of thermotical models, molecular simulations, and machine-learning approaches to elucidate the intricate relationship between composition, structure, and properties concerning polymer brushes in the context of nanotribology, surface hydration, and packing conformation. Upon acknowledging the challenges currently faced, we extend our perspectives toward future research directions by delineating potential avenues and unexplored territories. Our overarching objective is to advance our foundational comprehension and practical utilization of polymer brushes for antifouling applications, leveraging the synergy between computational methods and materials design to drive innovation in this crucial field.

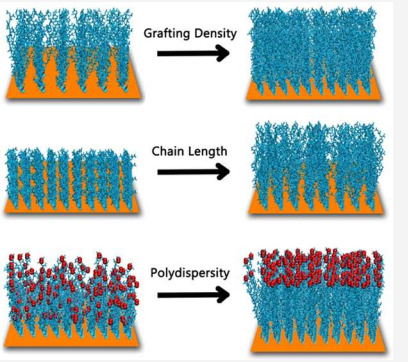

1. INTRODUCTION

Polymer brushes, also known as tethered bottlebrushes, represent a distinctive class of macromolecular structures characterized by a high dense grafting of polymer chains.[1−4] These chains are securely anchored onto diverse substrates, including inorganic and organic materials, metals, semiconductors, and biological substances. The anchorage of polymers to modify substrates can be accomplished through two primary processes: physisorption via noncovalent bond linkages and chemisorption via covalent bond linkages. Different physisorption methods (e.g., spin-coating, layer-by-layer assembly, solvent casting, and plasma deposition) and chemical anchorage techniques (e.g., grafting-to method, grafting-from method)[5−8] have been developed to cater a wide range of substrate shapes, including one-dimensional linear backbones, two-dimensional planar surfaces, and three-dimensional spherical or cylindrical matrices. The anchored polymer brushes enable the empowerment of a host substrate with a new spectrum of desirable properties, including enhanced thermal, mechanical, chemical, responsive, adhesive, and biocompatible characteristics.[9] These enhancements of surface functionality and property are achieved through meticulous modification of both polymer chains themselves, encompassing alteration in the chemical structure, hydrophobicity, charge distribution, and molecular weight, as well as the manipulation of surface properties, including surface-grafting density, thickness, roughness, patterning, and chain conformation. Additionally, the efficacy of polymer brushes is also affected by the methods employed for their synthesis and application. In essence, polymer brushes serve as a versatile toolbox in terms of surface modification, materials engineering, and tailored interactions for a wide range of scientific and industrial applications,[10] including membrane separation,[11] antifouling and antibacterial coatings,[12−16] (bio)sensors,[17] and cell culture and tissue regeneration.[18,19]

From a historical perspective, before the 1980s, early investigations into polymer brushes primarily centered on their fundamental physicochemical surface properties, such as wetting, friction, adhesion, corrosion resistance, and mechanical/thermal stabilization. Later, the emergence of advanced polymerization techniques, including ring opening metathesis polymerization (ROMP),[20] nitroxide-mediated polymerization

Received: October 25, 2023
Revised: December 15, 2023
Accepted: December 19, 2023
Published: December 28, 2023

https://doi.org/10.1021/acs.langmuir.3c03253
Langmuir 2024, 40, 1487−1502

(NMP),[21] atom transfer radical polymerization (ATRP),[22] single-electron-transfer living radical polymerization (SET-LRP),[23] and reversible addition−fragmentation chain transfer (RAFT) polymerization,[24] offer precise control over the chemical compositions and surface properties of tethered polymer chains, so polymer brushes have evolved into nanoscale soft building blocks. Consequently, research efforts have redirected their focus toward uncovering novel functionalities for polymer brushes,[25−27] including bioelectronics,[28,29] smart/responsive surfaces,[30−32] electrolytes and batteries,[33−36] (bio)catalysis,[37,38] and polymer-inorganic nanoparticles.[39−41]

Despite significant progress in polymer brushes through experiments, most of the findings have yielded only quasi-macroscopic properties and functionality. Molecular-level information, including uncertainties about the exact polymer chain conformation, bound solvents, and ions, remains unknown explicitly. The number of SCI-index papers on polymer brush studies between 2013 and 2023 reveals a stark contrast between computational and experimental research in this field (Figure 1). Theoretical modeling and molecular

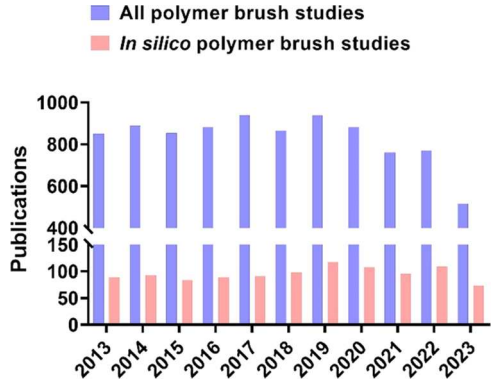

Figure 1. Number of SCI-index papers on polymer brush studies between 2013 and 2023, resulting from a search using keywords of "polymer brush" with or without "computation", "simulation", "modeling", and "in silico" in the topics of papers from the Web of Science database.

simulations have emerged as effective and indispensable tools for characterizing polymeric brush systems and gaining insight into the fundamental principles of molecular structures, (thermo)dynamics, and interactions that govern polymer brush properties. Pioneering theoretical research on polymer brushes, initiated by Alexander[42] and de Gennes,[43] closely paralleled experimental investigations. Single-chain mean-field theory (SCMFT) and its associated models (worm-like chain model, self-consistent field model) have been developed to elucidate the grafting density and conformation of polymer brushes.[44−46] SCMFT allows for the use of a simplified parameter, $\sum = \sigma\pi R_g^2$, to effectively describe and differentiate tethered polymer chains across three principal regimes: (1) the mushroom regime, characterized by highly flexible polymer chains ($\sum < 1$), (2) the crossover regime ($\sum \approx 1$), and (3) the brush regime, marked by highly stretched polymer chains ($\sum \gg 1$). This model not only elucidates the mushroom-to-brush transition from a single grafted chain to a polymer brush but also accounts for the influence of the solvent on grafting density in relation to this transition. However, recent experimental advancements in polymer brushes have introduced diverse polymerization techniques, notably grafting-to methods versus grafting-from methods, and more complex polymer architectures, such as multiblock polymers, branched polymers, and gradient polymers, particularly in stimuli-responsive systems. These new classes of polymer brushes pose challenges for SCMFT when characterizing tethered polymers using a single $\sum$ parameter, especially when obtaining or measuring the radius of gyration (R_g) of a tethered chain under specific experimental conditions can be difficult.

These polymer theoretical models, coupled with the majority of experimental techniques, can furnish only restricted atom-level insights into the conformational dynamics of brushes and their interactions with the environment. Molecular simulations, including molecular dynamics (MD), Monte Carlo (MC), dissipative particle dynamics (DPD), and Brownian dynamics (BD), have been conducted to study structural and thermodynamic properties of polymer brushes at coarse-grained[47−55] and atomic resolutions.[56−58] Different simulation approaches offer unique advantages in capturing various aspects of polymer brushes. Coarse-grained (CG) simulations excel in studying large polymer brush systems with long relaxation times associated with polymer dynamics. However, they may not accurately represent chemically specific interactions, such as hydrogen bonding. All-atomic MD simulations provide atomic-level details of equilibrium structures, dynamics, and interactions of polymer chains at lower free energy states but are limited by spatial and temporal constraints, typically in the nanometer and nanosecond range.[59] Monte Carlo (MC) simulations are particularly useful for studying chain growth processes akin to radical polymerization. However, they are often employed within implicit solvent models. More importantly, these simulations can serve as invaluable sources for establishing the composition−structure−property relationship of polymer brushes, which, in turn, can be used as critical inputs for machine-learning models. These data are essential for predicting and optimizing the structures and properties of new polymer brushes in an a priori fashion, greatly enhancing the design process. While modern computational modeling and simulations have greatly expanded our understanding of the fundamentals of polymer brushes, it is important to note that the specific selection of modeling parameters and methods can introduce variations in results or even discrepancies in the obtained data. Furthermore, investigating long-time and large-length-scale phenomena in polymer brushes and their associated systems still remains a challenging task due to limitations in accurate force fields.[60]

While there are several comprehensive reviews covering the experimental aspects of polymer brush synthesis, characterization, functionality, and applications, this review centers on the essential computational facets of polymer brushes throughout theoretical models, molecular simulations, and machine-learning approaches. In particular, we aim to understand the fundamental behavior of polymer chains with respect to their intrinsic chemical compositions and external surface packing properties at the molecular levels. Furthermore, the usage of machine-learning models will aid and enable the design of new polymer brushes. Taken together, the task of designing innovative polymer brushes that offer multifunctionality and precise control over surface properties continues to present significant challenges. This underscores the imperative for ongoing and collaborative efforts, combining comprehen-

https://doi.org/10.1021/acs.langmuir.3c03253
Langmuir 2024, 40, 1487−1502

sive simulations with experimental tests, for designing increasingly complex polymer brush systems.

2. STRUCTURAL CHARACTERIZATION OF POLYMER BRUSHES BY THEORETICAL MODELS

In the early pioneering computational studies of polymer brushes, polymer brushes are often described by the simple Alexander[42] or de Gennes[43,61] models in different solvent conditions, where the solvent is traditionally modeled by excluded-volume-type repulsive interactions between the individual monomeric units that form the polymer chains. Specifically, in a good solvent, a delicate equilibrium exists between repulsive and attractive forces among polymer chains, while in a poor solvent attractive forces tend to dominate. This intricate interplay between repulsion and attraction, stemming from both the enthalpic (interaction) and entropic (elastic) energy contributions of the polymer chains, has profound implications for the structure and dynamics of polymer brushes. As the grafting density increases, the spacing between the grafted polymer chains on the substrate becomes notably smaller than the average size of the free chains. So, steric hindrance and/or electrostatic repulsion forces compel the polymer chains to stretch themselves in the direction perpendicular to the surface. This leads to the adoption of brush-like conformations driven by minimizing intermolecular free energy throughout the entirety of the polymer brushes. This transition in conformation induced by grafting density signifies a shift from the "mushroom" regime, characterized by loosely packed and separated chains, to the "brush" regime, where the chains are densely packed and extend outward from the surface. Meanwhile, environmental factors, including pH, ionic strength, temperature, solvent, and salt types, exert a significant influence on the regulation of polymer brush conformational behavior. It is widely acknowledged, for instance, that charged polyelectrolyte brushes exhibit remarkable sensitivity, displaying intricate conformational shifts in reaction to fluctuations in ionic and solvent conditions. Interactions among ions, solvents, and polymers can either screen or induce interchain interactions, thereby triggering either the collapse or expansion of polymer chains within the brush.

In theory, the scaling and self-consistent-field (SCF) models[42,43,61] were initially introduced to elucidate the variations in thickness and density of polymer brushes across different regimes, considering factors such as grafting density, the degree of polymerization, and solvent quality. The excluded volume interactions among polymer chains, a key element in both the scaling method and self-consistent-field approaches, provide a reasonable description of the polymer brush thickness and density profile in good solvent conditions, in reasonable agreement with the computational predictions derived from both on- and off-lattice models. Regarding the grafting density effect, grafting density is defined as $\sigma = Np^2/A$, p represents the characteristic segment length of the polymer, N is the number of monomers in the chains, and A denotes the substrate area. There are three density regimes being identified for grafting polymer chains in good solvent (Figure 2): (1) at $\sigma < 0.004$, the brush exhibits characteristics of the mushroom regime; (2) In the range of $0.01 < \sigma < 0.05$, the brush adheres to the scaling behavior as predicted by SCF theory, resulting in parabolic monomer density profiles; and (3) at $\sigma > 0.05$, the brush behavior diverges from the predictions of the SCF theory, leading to the flattening and stretching out of density profile.[62] In quantitative terms, these models have revealed a scaling relationship between the height (h) of a brush under conditions of a good solvent and its grafted chain length (N) and surface coverage density (σ), as expressed by $h \sim N\sigma^{1/3}$. In particular, these models predict a typical monomer density profile characterized by a parabolic dependence at low grafting density[63] and a step function at higher grafting densities.[42] In these regimes, the conformation of the polymer chains is influenced by factors such as the grafting density, chain length, and interaction between monomers. In both the mushroom and brush regimes, polymer entanglement is generally less likely. In the mushroom regime, polymer chains are less densely packed and are separated by large distances; thus, the chains do not experience significant overlap or entanglement. In the brush regime, polymer chains extend away from the surface due to strong steric repulsive forces between chains. This steric repulsion tends to repel chains from each other and keeps them from retaining a more ordered and extended configuration, which helps to reduce the likelihood of interpenetration or entanglement between adjacent chains. However, under conditions where the grafting density is high or the chains are long, there might be some degree of overlap or entanglement. This situation could be more prevalent in the crossover regime, where there is a transition from a brush to a denser, more entangled state.

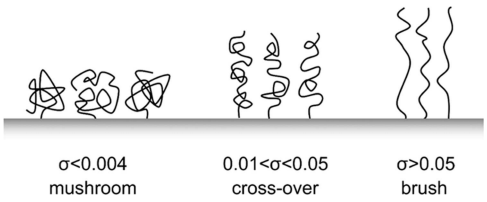

Figure 2. Tethered polymer chains across three principal regimes, including a mushroom regime, characterized by highly flexible polymer chains (σ<0.004), a crossover regime ($0.01 < \sigma < 0.05$), and a brush regime, marked by highly stretched polymer chains ($\sigma > 0.05$). σ (grafting density) = Np^2/A, p represents the characteristic segment length of the polymer, N is the number of monomers in the chains, and A denotes the substrate area.

However, there exist some differences in the density distribution of individual monomers and free chain ends of grafted polymers in the direction perpendicular to the grafting plane when comparing scaling approaches,[42] Flory-type approaches,[43] and SCF approaches.[45] Both scaling and Flory-type approaches utilize a step function to depict the monomer density distribution. This function linearly decreases to zero as one moves from the substrate ($h = 0$) to the top of the brush. In contrast, SCF theory exhibits a parabolic dependence of monomer density on the distance from the grafting surface, which diminishes at the brush height.[63] Regarding the free ends of grafted polymers, the scaling approaches predict that these free chain ends are exclusively situated at the forefront of the brush layer. Conversely, the SCF theory posits that the free ends of grafted polymers exhibit a nonzero probability distribution throughout the brush, which starts with a linear increase, followed by a faster decay after reaching a maximum at $h/\sqrt{2}$, ultimately reaching a zero value at h. Unlike scaling-based theories, single-chain mean-field theory (SCMF) explicitly considers intramolecular and surface interactions between polymers and proteins, while it models intermolecular interactions by using a mean-field approximation. This approach allows for the inclusion of detailed conformational

https://doi.org/10.1021/acs.langmuir.3c03253
Langmuir 2024, 40, 1487−1502

Table 1. Survey of Molecular Simulations for Investigating the Physicochemical Properties of Representative Polymer Brushes

polymer brush	properties	models and force fields	ref
PDMAEMA and PMETAC	swelling/collapsing property of brushes in response to pH, solvent, and salts	all-atom MD simulations with GROMOS force field	84
Lennard–Jones beads	dynamics of bead-like brushes in response to solvent and grafting density	coarse-grained MD simulations with bead–spring model for polymers and point-like particles for solvent	47
lattice and off-lattice chains	structure and dynamics of point-like brushes both on and off the lattice in response to grafting density, chain length, and temperature	Monte Carlo simulations with bond-fluctuation lattice model and off-lattice model for polymer chains	73,56
polystyrene	structure and dynamics of highly dense polystyrene brushes in benzene as a good solvent	MARTINI CG model for polystyrene	48
dextran	friction of dextran brushes against the wall under different shear speeds	CG, multibead spring model for dextran brushes in an implicit solvent	49
polystyrene–poly(ethylene oxide) mixed brush	brush height of polystyrene–poly(ethylene oxide) mixed brushes in response to solvent and grafting density	CG, multibead spring model for mixed brushes in an implicit solvent	51
bead–spring chains	chain stiffness effect on the properties of topological polymer brushes in a good solvent	LAMMPS CG model for general polymer chains in an implicit solvent	50,77
bead–spring chains	friction between two polymer brushes under shear in a good solvent	Kremer–Grest, CG-bead model of polymer brushes in explicit LJ dimer solvent	86
bead–spring chains	compression and friction of polymer brush in response to grafting density, shear rate, and solvent	off-lattice bead–spring model for polymer chains using grand-canonical-ensemble MD simulations, MD simulations, or DPD simulations	87–90
poly(ethylene oxide)	conformation and thickness of PEO brushes as a function of the chain length and coverage density	all-atom, explicit-water MD simulations with the CHARMM force field or quantum chemistry-based force field	56,80
deblock dimethylmethylacrylamide-methacrylic acid	ionic effects on the interfacial structure and mechanics of a polyelectrolyte brush	all-atom, explicit-water MD simulation with OPLS-AA force field	58
oligopeptide-tethered PEG	pH-responsive conformational change of charged oligopeptide-tethered PEG brushes in response to charged residue sequences and compositions	all-atom, explicit-water MD simulation with Gromos force field	85
zwitterionic sulfobetaine and carboxybetaine	hydration structure and antifouling properties of sulfobetaine and carboxybetaine brushes at different grafting densities and in the presence of different types of ions	all-atom, explicit-water MD and steered MD simulations with OPLS force field	98,99
poly(*N*-hydroxyalkyl acrylamide), poly(carboxybetaine methacrylate), poly(sulfobetaine methacrylate), poly((2-(methacryloyloxy)ethyl) phosporylcoline)	packing structure, surface hydration, and protein resistance of four poly(*N*-hydroxyalkyl acrylamide) (PAMs) brushes with different carbon spacer lengths and three zwitterionic brushes with different pendant groups	all-atom, explicit-water MD and steered MD simulations with CHARMM force field	103,104
peptoids	conformation and hydration properties of a series of zwitterionic "peptoids" brushes at different grafting densities	all-atom, explicit-water MD with Gromacs force field	102

https://doi.org/10.1021/acs.langmuir.3c03253
Langmuir 2024, 40, 1487−1502

and chemical information on the molecules by accurately representing the single-chain conformations. A number of SCMF studies have successfully predicted the protein adsorption amount on the grafted PEO-based brushes with varied PEO chain lengths and surface chain density.[64−66] They discovered that PEO attached to a hydrophobic surface decreased protein adsorption by obstructing protein adsorption sites. According to the SCMF model, although surface density played a significant role in preventing protein adsorption, chain length had a relatively minor impact on protein adsorption. As a result, the SCMF model is effective in explaining experimental outcomes involving short PEO chains ($n < 20$).

These theoretical models, primarily employed in the realms of continuum scaling fields and self-consistent fields, have provided initial and significant insights into the conformational dynamics of polymer brushes in relation to grafting density, chemical composition, and external factors (e.g., pH and salt types). However, all of these models come with several inherent limitations. First, while scaling-based continuum models and SCF models can effectively describe the conformations and concentration profiles for most practical systems containing neutral chains with $N < 20$ (N monomers per chain) at any given grafting density (σ), they often encounter difficulties in understanding the conformation of long chains ($N \geq 100$) and polyelectrolyte chains. Second, polymer brushes are constructed using structureless chains, and this construction assumes that the coverage density is high enough to ensure that the size of the thermal blobs is larger than the distance between grafting points. This assumption may not hold true for the practical use of polymer brushes with lower surface densities. Third, these models employ an implicit representation of solvents (such as water, alcohol, and others), which provides a simplified depiction of the complex interactions among polymer chains, solvents, and salts across a range of environmental conditions. Solvent quality as an important factor is at best approximated through a Flory−Huggins-type enthalpic term. Additionally, excluded volume interactions are primarily designed to describe polymer interactions in good solvents. These inherent limitations contribute to unresolved disparities that persist between the results from these theories and experimental observations, particularly regarding the dynamic behavior of polymer brushes in poor solvent conditions.

3. MOLECULAR SIMULATIONS OF POLYMER BRUSHES

To clarify from a molecular simulation perspective, while both polymer brushes and self-assembled monolayers (SAMs) involve molecules attached to a substrate, the distinction between polymer brushes and SAMs lies in the nature of their molecular arrangement.[67−71] Polymer brushes exhibit a more extended and multilayered structure compared with the compact, single-layer formation of SAMs. Polymer brushes involve extended polymer chains often arranged in multiple layers, providing greater flexibility. In contrast, SAMs consist of a single layer of molecules spontaneously organized on a substrate. SAMs form a closely packed, well-ordered monolayer composed of smaller molecules with fewer repeating units. The coverage of SAMs is uniform, lacking the extended protrusions seen in polymer brushes. Below, the discussion exclusively focuses on molecular simulations of polymer brushes (Table 1).

3.1. Conformational Properties of Polymer Brushes.

Generally speaking, the evolution of molecular simulations for polymer brushes, taking into account the computational resource requirements and the necessity for force field development, can be traced from the historical use of bead−spring models for polymer chains in implicit solvent to coarse-grained (CG) models that represent both polymer chains and solvents, to CG models focusing solely on polymer chains in an explicit solvent, and ultimately to all-atom models for both polymer chains and solvents.[60,72] Therefore, molecular simulations with atomistic or coarse-grained models can offer a complementary perspective on the behavior and structure−property relationships of polymer brushes by manipulating the number of segments and molecular architectures of the grafted polymer chains, the coverage densities of modified surfaces, and the interactions of monomers with surface, temperature, and solvent quality, in comparison to the theoretical models mentioned above.

In the early investigations of grafted polymer brushes, Monte Carlo (MC) simulations, utilizing both the bond-fluctuation lattice model[73] and the off-lattice model,[74] revealed the dynamic behavior of polymer chains within a brush regime (Figure 3a1). Specifically, the end groups of polymer chains did not exhibit strictly linear-like stretching-out conformations perpendicular to the surface. Instead, the chains displayed large fluctuations resembling random walks, although such structural fluctuations in polymer chains decreased as both chain length and grafting density increased. On the other hand, as temperatures decreased, the solvent quality shifted from good to poor, causing the polymer chains to stretch less and the brush thickness to collapse. In pursuit of a more realistic modeling approach for polymer brushes that incorporates explicit solvent effects, coarse-grained (CG) models were developed by employing a bead−spring representation for polymer chains and a single-point model for solvent. By varying the interaction parameter (ε) in the Lennard−Jones potential function, it becomes possible to finely adjust the pairwise interactions between polymer−polymer, polymer−solvent, and solvent−solvent, spanning from repulsive forces to attractive ones. This also allows us to examine four distinct scenarios that describe the conformations of polymer chains under varying solvent conditions and grafting densities. At either low grafting densities or in a bad solvent, bead brushes develop considerable lateral inhomogeneity, primarily due to dimple formation[47] (Figure 3a2), consistent with the results from the on- and off-lattice polymer brushes.[73,74] Conversely, at high grafting densities in a good solvent, bead-like polymer chains underwent a pronounced stretching from the grafting surface, forming a characteristic brush structure. However, in the case of a dense brush in a poor solvent, the top layer of polymer chains exhibited an almost random orientation. This particular scenario has also been observed in experimental studies of grafted polymers in a poor solvent.[75,76] Furthermore, the stiffness of polymer chains also exerts a notable influence on the dynamic properties, especially in the case of polymer chains with nonlinear topological structures, such as branched or ring structures, when subjected to compression[50,77] (Figure 3a3). MD simulations conducted on compressed polymer brushes containing rings have revealed that stiff polymer chains with shorter persistence lengths tend to be penetrated by linear free chains. This penetration occurs due to a combination of conformational entropy penalties and a lower monomer density within the brushes. However, when the persistence

https://doi.org/10.1021/acs.langmuir.3c03253
Langmuir 2024, 40, 1487−1502

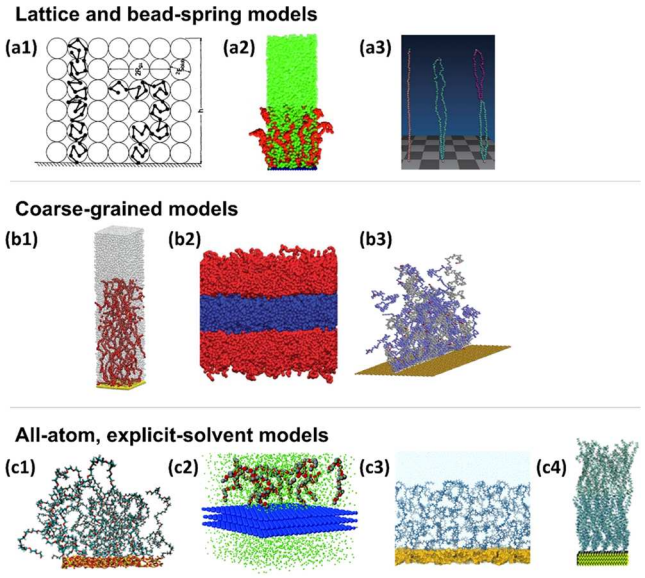

Figure 3. Typical simulation models and molecular simulations showcasing the conformational changes of polymer brushes at lattice/bead−spring, coarse-grained, and atomic resolutions in the presence of an explicit or implicit solvent. (a1) MC simulations of generic polymer brushes at different grafting densities using the bond-fluctuation lattice model and implicit solvent. Reproduced with permission from ref 73. Copyright [1991] [American Institute of Physics] (a2) MD simulations of generic polymer brushes using the bead−spring model in an explicit point-like solvent. Reproduced with permission from ref 47. Copyright [2007] [American Institute of Physics] (a3) MD simulations of ring polymer brushes with different topological chain structures using bead−spring model and implicit solvent. Adapted with permission from ref 77. Copyright [2016] [Chinese Physical Society and IOP Publishing Ltd.]. (b1) MD simulations of MARTINI coarse-grained polystyrene brushes in an explicit bead-like benzene solvent. Reproduced with permission from ref 48. Copyright [2012] [American Chemical Society]. (b2) MD simulations of MARTINI coarse-grained poly(ethylene glycol) brushes in an implicit water solvent. Reproduced with permission from ref 78. Copyright [2009] [American Chemical Society]. (b3) MC simulations of the growth of coarse-grained polymer brushes from flat surfaces. Reproduced with permission from ref 79. Copyright [2017] [Elsevier Ltd.]. Atomic MD simulations of (c1) neutral poly(ethylene oxide) brushes on a siloxane surface in explicit TIP3P water. Reproduced with permission from ref 56. Copyright [2011] [American Chemical Society]. (c2) neutral poly(ethylene oxide) brushes on a graphite surface in explicit TIP4P water. Adapted with permission from ref 80. Copyright [2011] [American Chemical Society]. (c3) charged poly(2-(methacryloyloxy)ethyl trimethylammonium chloride) brushes on silicon in SPC water in response to changes in pH, solvent, and salt types Reproduced with permission from ref 84. Copyright [2019] [American Chemical Society]. (c4) charged diblock copolymer brushes consisting of dimethylmethylacrylamide (DMMAA) and methacrylic acid (MAA) on a hydroxylated silicon (100) surface in SPC/E water and different ions. Reproduced with permission from ref 58. Copyright [2013] [The Royal Society of Chemistry].

length (i.e., stiffness) is held constant, compression on both ring-containing polymer brushes and linear polymer brushes did not lead to significant differences in terms of changes in brush height and bending energies within the polymer brushes. This suggests that the topological structures are less sensitive to brush structures and the penetration of free polymer chains into the brushes when the stiffness remains consistent.

In contrast to the bead−spring model for polymer brushes, which loses chemical specificity, an enhanced MARTINI coarse-grained (CG) model was developed to represent real polystyrene brushes immersed in benzene, a good solvent, within a high grafting density regime[48] (Figure 3b1). While all polystyrene brushes fell within the high-density regime, only the brush with the highest density displayed the characteristic fully stretched-out conformation, with its chain ends moving away from the grafting surface. In the case of other high grafting densities, some brush chains exhibited different tilt angles and experienced deep penetration of the chain ends into the brush. This indicates that achieving fully stretched configurations, even under a high grafting density, is a relatively rare event. Instead, the titled polymer chains represent the most energetically favorable stretched configurations in metastable states, transiting from a semicollapsed state to a fully extended one. In another set of coarse-grained molecular dynamics simulations involving PEO or PEG brushes grafted onto a hydrophobic surface[78] (Figure 3b2), as the distance between neighboring PEG chains decreased (corresponding to an increase in grafting density), the simulations accurately replicated a structural transition from a mushroom regime to a brush regime. This transition was evidenced by the reduction in the effective lengths of PEG brushes, which closely aligned with the predictions of Alexander−de Gennes theory. However, extending the applicability of PEG brushes from hydrophobic surfaces to PEG brushes grafted on lipid bilayers (PEGylated bilayers) necessitates the further development of force fields. Regarding the solvent effect, CG MD simulations conducted on mixed polymer brushes composed of polystyrene−poly(ethylene oxide) (PS−PEO) have revealed that PS predominantly determines the thickness of these PS−PEO mixed polymer brushes across various solvents and grafting densities.[51] From the perspective of algorithm development, a hybrid approach combining Monte Carlo simulation and a dynamic lattice liquid (DLL) model has been devised to replicate the growth of coarse-grained (CG) polymer brushes from a flat surface, akin to atom transfer radical polymerization (ATRP)[79] (Figure 3b3). By the adjustment of the reaction probability and grafting density, this algorithm allows for the regulation of polymerization rates, resulting in the formation of both dense and moderately dense brushes with degrees of polymerization ranging from 45 to 150.

Although CG simulations provide accelerated dynamic responses in polymer brushes and other materials by reducing the degrees of freedom in the studied systems, it is essential to note that CG models also reduce fluctuating and frictional forces linked to configurational entropy, which is inevitably lost to some extent when compared to atomistic models.[53] All-atom, explicit-water molecular dynamics (MD) simulations of poly(ethylene oxide) (PEO) brushes have been conducted to investigate their response to molecular weight and coverage density[56,80] (Figure 3c1,c2). At low surface coverages, PEO chains adopt curly three-dimensional mushrooml-ike conformations, consistent with a scaling analysis, which predicts PEO chains with a scaling exponent smaller than 3/4, as derived for a free two-dimensional coil in a good solvent. At high surface coverages, PEO chains form well-defined, extended brush-like structures. This transition is primarily driven by strong dispersion interactions between the PEO chains. The brush-like conformation arises from a combination of factors: the loss of entropy due to reduced degrees of

https://doi.org/10.1021/acs.langmuir.3c03253
Langmuir 2024, 40, 1487−1502

freedom in the stretched chains, spatial confinement, and the gain of negative enthalpy resulting from the reduction in excluded volume interactions between chains. Furthermore, these atomistic simulations yielded PEO brush thicknesses of 2.2 and 5.9 nm for 12 and 45 EO monomers, respectively. These results are in excellent quantitative agreement with experimental measurements of 2.8 ± 0.1 and 7.5 ± 0.3 nm for the same monomers,[81] as well as with the range of 3.957−4.835 nm obtained from coarse-grained MD simulations of PEO brushes with 40 EO monomers.[82]

In contrast to neutral polymer brushes, polyelectrolyte brushes display a more intricate and adaptive behavior, primarily driven by their inherent charge and remarkable sensitivity to ionic environments.[83] When subjected to ionic surroundings, such as the presence of salts or pH variations, polyelectrolyte brushes can undergo substantial transformations in terms of their conformation, swelling, and height. Notably, these changes arise from electrostatic interactions between the charged polymer chains and the ions in the solution, leading to either repulsion or attraction forces that profoundly affect the brush volume. For instance, polyelectrolyte brushes can exhibit significant swelling or deswelling behavior, a phenomenon attributed to the interplay of electrostatic interactions with ions in the solution. In low ionic strength environments, these brushes tend to stretch out due to reduced ionic screening effects, assuming elongated conformations. Conversely, in high ionic strength solutions, the brushes tend to collapse, driven by increased ionic screening, and adopt more compact conformations. One crucial departure from neutral brushes in good solvents, which exhibit a height proportional to the chain length (N) and the grafting density (σ) following the Alexander−de Gennes relation of $h \sim N{\cdot}\sigma^{1/3}$, is that the height of polyelectrolyte brushes remains independent of the grafting density (σ) but depends on the salt concentration in the surrounding medium. This distinction arises because the charge density of polyelectrolyte brushes, influenced by the ionic environment, has a more dominant effect on their height than does the grafting density.

Poly(dimethyl aminoethyl methacrylate) (PDMAEMA) and poly(2-(methacryloyloxy)ethyl trimethylammonium chloride) (PMETAC) brushes, representing respective weak and strong polyelectrolytes, were modeled and simulated to differentiate the swelling/collapsing behaviors in response to changes in pH, solvent, and salt types using MD simulations with GROMOS-derived force field[84] (Figure 3c3). Notably, PDMAEMA brushes, classified as weak polyelectrolytes, exhibited the characteristic swelling at low pH but collapsed to near-dry states at higher pH levels. Compared to the weak PDMAEMA brushes, which do not exhibit strong salt- and solvent-responsive behavior, the strong polyelectrolyte PMETAC brushes displayed greater sensitivity to both solvents and salt types. PMETAC brushes underwent large conformational changes, transiting from a swelling and stretching state in water (considered a good solvent) to a collapsed state in cyclohexane (considered a poor solvent). Additionally, they exhibited an increase in swelling in kosmotropic salts of NaCl and Na_2SO_4 while experiencing a decrease in swelling when exposed to chaotropic $NaClO_4$. The swelling behavior of polyelectrolyte brushes can be attributed to their pronounced swelling in aqueous solutions, primarily driven by hydration and electrostatic repulsion between polymer chains. Conversely, the collapsing behavior in apolar solvents is primarily a consequence of the ionic screening effect.

Additionally, atomic MD simulations were employed to investigate the salt-responsive mechanical and structural properties of diblock polyelectrolyte brushes composed of dimethylmethylacrylamide (DMMAA) and methacrylic acid (MAA)[58] (Figure 3c4). The introduction of smaller cations such as Li^+ and Na^+ resulted in the formation of rigid and uniformly packed PDMMAA-*b*-PMAA brushes characterized by a distinct and well-defined brush/water interface. On the other hand, the presence of larger ions such as K^+, Rb^+, and Cs^+ induced a significant approximately 5-fold increase in the compressibility of the diblock brushes, leading to a parabolic brush/water interface. These differences in structure were attributed to variations in the strength of the salt bridge network formed between the cationic species and the carboxylic groups within the different MAA blocks. These structural distinctions are closely related to the mechanical properties exhibited by these polyelectrolyte systems. Additional MD simulations were conducted to explore the conformational changes of pH-responsive charged polypeptides tethered to poly(ethylene glycol) (PEG) brushes. These simulations aimed to investigate how different charged sequences, compositions, and lengths, including lysine (K), glutamic acid (E), and histidine (H) residues, impact the conformational behavior of these brushes.[85] The presence of both E and K, with K located at the exposed end and E at the tethered end of the peptide, along with an effectively "neutral spacer" in the form of an EK block within the large block of H residues, can induce folding in the unprotonated state due to favorable electrostatic interactions between K^+ and the PEG brush. A high grafting density of long (20mer) PEG chains adjacent to short (5mer) PEG chains, in proximity to the (10mer) PEG-tethered peptide, resulted in a decrease in the pH-responsive shielding and exposure of the oligopeptide in most sequences due to the dense packing of long PEG chains, which intensified interactions with the positively charged regions within the peptide sequence.

3.2. Nanotribology Properties of Polymer Brushes. In addition to the extensively studied properties associated with the conformational changes of polymer brushes, the nanotribological characteristics of these brushes represent another crucial aspect that has garnered significant attention through numerous molecular simulations.[49,86,87] Numerous simulations have been conducted to investigate sheared polymer brushes, employing various modeling approaches such as bead−spring models,[87−90] coarse-grained (CG) models,[86] and all-atom models,[91,92] as well as different solvent treatments, including the implicit DPD thermostat, the self-consistent solution of the Brinkman equation, or the explicit inclusion of solvent molecules in various thermodynamic ensembles. These computational studies have revealed a consistent trend: a strong frictional response in poor solvent conditions, likely due to monomer−monomer attractions, but a considerably weaker shear force in good solvents. In the case of polymer brushes in good solvents, which is the most common scenario, high shear rates lead to a significant reduction in friction. This reduction is closely associated with a corresponding decrease in the thickness of the polymer brush and a decrease in the interpenetration of chains between the brushes, i.e., the extent to which the opposing brushes overlap. As a result, the stretching chains due to the sliding velocity ultimately diminish the interactions between the opposing brushes in the region of

https://doi.org/10.1021/acs.langmuir.3c03253
Langmuir 2024, 40, 1487−1502

reduced overlap. Of particular significance, in a good solvent there always exists an atomic-level thin solvent layer within the interfacial region between the brushes. This layer further contributes to enhanced lubrication between the brushes.

While steady-shear simulations of polymer brushes generally exhibit qualitative agreement with experimental observations, it is essential to recognize that the tribological responses of polymer brushes can significantly differ for polymers with long chains and high grafting densities. In molecular simulations, polymer chains are typically quite short, often consisting of only N = 20−50 monomers. These short chains do not experience entanglement under shear or compression forces. Consequently, extending the correlation between friction and shear rates to polymer brushes with longer chains and higher grafting densities presents challenges. In cases of long-chain grafting polymer brushes, their shear behavior is likely linked to a mechanism involving sliding-induced chain "stretching and disentanglement" (Figure 4a). In the case of long-chain

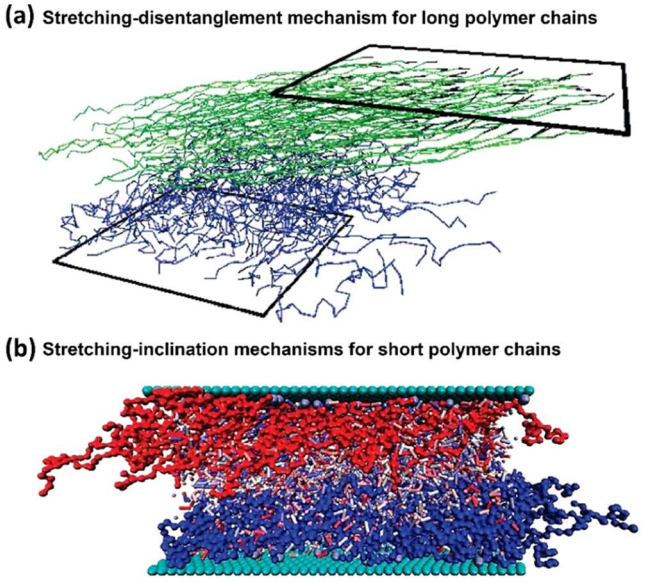

Figure 4. Typical simulation models and molecular simulations showcasing the two shear mechanisms between polymer brushes. (a) The stretching−disentanglement mechanism for long polymer chains. Reproduced with permission from ref 88. Copyright [2001] [American Chemical Society] and (b) stretching−inclination mechanisms for short polymer chains Reproduced with permission from ref 86. Copyright [2010] [American Chemical Society], both occurring between two opposing polymer brushes in good solvent under different shear rates.

polymer brushes, a stick−slip motion can manifest as a result of entropic forces, leading to enhanced dissipation. This occurs because the interdigitation of the brushes strives to disentangle the polymer chains and return the system to equilibrium before relaxing the grafted chains.[91] On the other hand, if the polymer relaxation time is significantly longer than the entanglement time scale, brush systems would be considerably distant from thermal equilibrium, which could result in large fluctuations in friction or even mechanical instability of the brush systems.[92] In contrast, short chains may be more appropriately associated with a "stretching and inclination" mechanism (Figure 4b). In such cases, scaling theory emerges as a more appropriate choice, particularly when dealing with short chains, semidilute brushes. MD simulations of strongly compressed, non-entangled polymer brushes revealed that an increase in chain length and grafting density led to a larger frictional force per chain. This behavior manifests as a linear relationship between friction and a wide range of compressions and shear rates.[86]

3.3. Hydration Properties of Polymer Brushes. It is generally accepted that surface hydration, along with steric repulsion, has been proposed as the key nonfouling mechanism of polymer brushes and other coating materials.[93−95] Over decades of research, compelling evidence from both experimental and theoretical studies has consistently demonstrated that interfacial water near polymer-grafted surfaces exhibits distinct characteristics. This interfacial water layer extends to tens of nanometers from the surface and exhibits significant distinctions, not only in terms of its structure, dynamics, and binding affinity when compared to the behavior of bulk water but also in terms of the altered surface properties, including wettability, adhesion, friction, and biocompatibility. A robust hydration layer formed at the polymer/water interface serves as both a physical and energetic barrier, effectively preventing foulant adsorption onto the polymer-grafted surfaces. The expulsion of water molecules from the interfacial region between polymers and foulants requires strong surface interactions with foulants to compensate for the loss of solvent entropy during foulant adsorption. However, the formation of a tightly bound hydration layer at the polymer interface can be achieved by different mechanisms. Hydrophilic polymers achieve surface hydration through hydrogen bonding interactions (Figure 5a), while zwitterionic polymers achieve hydration via ionic solvation (Figure 5b). The strength of surface hydration primarily depends on the physicochemical properties of the materials themselves, including their chemical structure, hydrophobicity, charge distribution, and molecular weight, as well as their surface packing characteristics, such as packing density, film thickness, roughness, and chain conformation.

Atomistic molecular dynamics (MD) simulations were performed on PEO brushes to explore the variations in surface hydration with changing grafting density.[57] Increasing the grafting density led to several notable changes in PEO chains being extended farther away from the surface, a loss of hydration, and a step-like density profile with the brush height aligning with the expected $\sigma^{1/3}$ scaling. Additionally, the mobility of PEO-bound water and PEO tails decreased significantly as the grafting density increased, indicating that strong surface hydration in a dense PEO brush plays a pivotal role in resisting the adsorption of foulants onto the PEO-grafted surfaces. Likewise, steered MD (SMD) simulations involving alginate foulants approaching PEG-grafted membranes showcased the emergence of robust repulsive forces between the foulant and the membranes. These forces stemmed from the compression of the hydration layer and were observed consistently across various surface chemistries and grafting densities, affirming the effective antifouling properties of the system.[96] Furthermore, MD and SMD simulations of PVDF-*g*-DMAPS brushes in the presence of explicit water revealed the existence of the hydration layer at the water/membrane interface. This hydration layer exhibited heightened hydrogen bonding (HB) strength and electrostatic repulsion, which played a dominant role in imparting antifouling properties to the system.[97]

The relationship between the grafting density and surface hydration in polymer brushes is rather intricate. Several studies employing protein adsorption assays have demonstrated that a

https://doi.org/10.1021/acs.langmuir.3c03253
Langmuir 2024, 40, 1487−1502

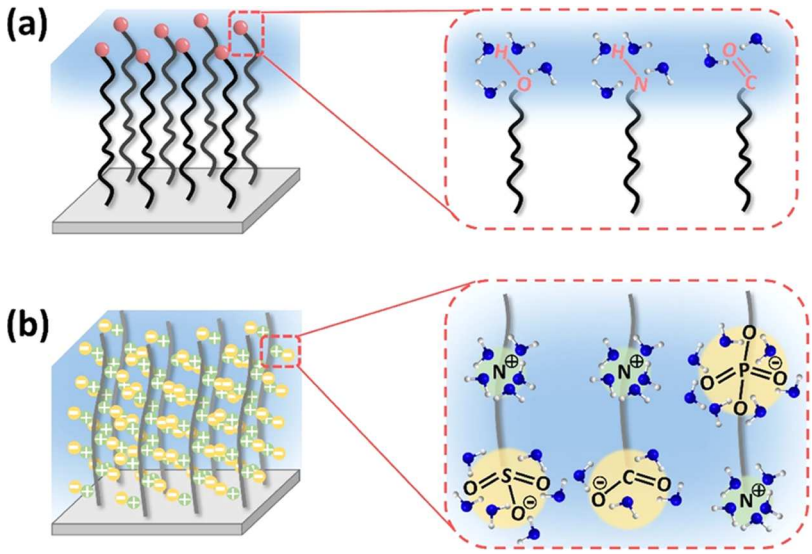

Figure 5. Surface hydration mechanisms of neutral hydrophilic and zwitterionic polymer brushes: (a) hydrophilic polymer brushes achieve surface hydration through hydrogen bondings, while (b) zwitterionic polymer brushes achieve hydration via ionic solvation.

relatively high grafting density is typically necessary to effectively inhibit protein adsorption. However, an excessively high grafting density may not always be the optimal choice for protein adsorption inhibition. It is only at an optimal high grafting density that polymer brushes exhibit remarkable resistance to protein adsorption from different biological media (including undiluted blood plasma and serum and whole blood), ultimately resulting in nearly undetectable protein adsorption. To unravel this seemingly counterintuitive antifouling behavior, MD simulations have revealed that at the optimal grafting density, water molecules can still penetrate and remain within the brush region by forming a robust hydrogen-bonded network with polymer chains. This is supported by the prolonged residence time of hydrogen-bonded water molecules, which serves as an indicator of enhanced surface hydration that contributes to the improved antifouling properties of the polymer brushes. Conversely, at extremely high grafting densities, polymer volume fraction increases and dispersion interactions between polymer chains take precedence, which causes not only the stretching of polymer chains but also the expulsion of water molecules from inside brushes to the surrounding environment. Such dehydration of polymer chains further enhances dispersion interactions, making the chains even more rigid. As a result, highly dehydrated, stretched, and less flexible chains compromise surface hydration due to the reduction of interfacial energetics concomitant with the replacement of water molecules at the surface by adsorbed solutes. This alteration in surface hydration ultimately impacts the antifouling properties of polymer brushes.[57]

Steered MD simulations with umbrella sampling have reported that zwitterionic sulfobetaine brushes exhibit distinct antifouling mechanisms depending on their grafting density.[98] At higher grafting densities, sulfobetaine brushes adopt a more organized structure capable of retaining a tightly bound hydration water layer at the interface. This water layer acts as both a physical and energetic barrier, effectively preventing foulant adsorption. In contrast, lower grafting density brushes exhibit randomly oriented structures, resulting in steric repulsion, which is the primary mechanism responsible for surface resistance to foulants. This difference in structure and behavior highlights the grafting-density-dependent nature of the antifouling properties of polymer brushes. Moreover, carboxybetaine brushes exhibited a stronger association with small ions of Li^+ and Na^+, whereas sulfobetaine brushes showed a higher affinity for larger ions of K^+ and Cs^+.[99−101] The introduction of these ions at intermediate and low grafting densities disrupted the association of the zwitterionic branches, causing the polymers to adopt a randomly oriented and dispersed branch configuration with considerable swelling. Similarly, zwitterionic "peptoids" brushes elevated chain flexibility and increased water density surrounding the chains at low and intermediate grafting densities, but at high grafting densities, these effects were suppressed due to free volume effects.[102] This structural change compromises surface hydration and brush-like structure, thus leading to a reduction in their antifouling efficacy. Therefore, in addition to surface hydration, other factors contributing to antifouling performance include high chain mobility, the presence of a large exclusion volume, and the steric repulsion offered by the polymer brushes. These elements collectively play a role in the antifouling properties of materials.

It is important to highlight that those molecular simulations of polymer brushes often lack accurate packing structure information, especially for widely used antifouling polymers grafted onto gold substrates. These simulations typically assume a conventional $\sqrt{3}\times\sqrt{3}$R30o lattice structure for polymer chains with a chain−chain separation distance of 4.95 Å. However, this packing structure oversimplifies the reality, neglecting variations in chain size, chemistry, and orientation. To address this issue, molecular mechanics simulations were carried out for a series of polymer brushes, including four poly(*N*-hydroxyalkyl acrylamide) (PAMs) brushes with different carbon spacer lengths (CSLs = 1, 2, 3, and 5) and three zwitterionic polymer brushes of poly(carboxybetaine methacrylate) (pCBMA), poly(sulfobetaine methacrylate) (pSBMA), and poly((2-(methacryloyloxy)ethyl) phosporylcoline) (pMPC). These brushes adopted different packing structures, each characterized by distinct unit cell dimensions for pHMAA (a = 8.652 Å, b = 4.995 Å, γ = 90°),

https://doi.org/10.1021/acs.langmuir.3c03253
Langmuir 2024, 40, 1487−1502

pHEAA (a = 8.652 Å, b = 4.995 Å, γ = 90°), pHPAA (a = 9.990 Å, b = 5.768 Å, γ = 90°), and pHPenAA (a = 11.536 Å, b = 4.995 Å, γ = 90°),[103] as well as for pCBMA (a = 10.395 Å, b = 7.630 Å, γ = 65.2°), pSBMA (a = 14.980 Å, b = 7.630 Å, γ = 48.2°), and pMPC (a = 11.360 Å, b = 8.652 Å, γ = 61.6°).[104] A combination of MD and SMD simulation studies further revealed that pHMAA and pHEAA with shorter CSLs (CSLs = 1−2) exhibited stronger and more stable interactions with water molecules than pHPAA and pHPenAA with longer CSLs (CSLs = 3 and 5). This CSL-induced strong surface hydration on pHMAA, pHEAA, and pHPAA brushes contributed to their high resistance to lysozyme adsorption, in stark contrast to the behavior of lysozyme adsorption on pHPenAA brushes.[103] Among the zwitterionic brushes, all of which exhibited strong surface resistance to lysozyme adsorption, the repulsive forces acting on lysozyme varied in the following order: pCBMA > pMPC > pSBMA > PEG, consistent with the order of surface hydration.[104] These computational studies highlight how even subtle structural changes in hydrophilic pendant groups within the same polymer backbone can significantly enhance antifouling performance. These studies offer valuable insights into structure-based design principles, suggesting that the strategic combination of hydrophilic or zwitterionic groups with optimal CSLs represents a promising structural motif for the development of novel and highly effective antifouling materials, extending beyond conventional ethylene glycol-based antifouling materials.

In addition to surface hydration, the concept of "steric repulsion", which is derived from colloid stability theory, also plays a vital role in preventing surface fouling, especially in the case of long-chain polymers.[13,105] When foulants approach and compress long polymer chains, repulsive forces come into play, preventing foulant adsorption due to the unfavorable decrease in entropy. In contrast to short-chain polymer brushes or self-assembled monolayers, where surface hydration is the primary driver of foulant resistance,[67] long-chain polymer brushes rely on both surface hydration and steric repulsion working together to achieve the highest level of nonfouling ability. It should be noted that conventional steric repulsion theory, based on the polymer brush model, is not applicable to the adsorption of rigid proteins such as albumin, heparin, or dextran on hydrophobic surfaces.[65] Furthermore, experimental factors such as enhanced chain mobility and significant exclusion volume are also contributors to their antifouling performance.[14,93] Theoretical analysis reveals two distinct modes of protein adsorption on polymer brushes, wherein proteins are represented as structureless colloidal particles and polymers are treated as simple flexible chains.[46] Primary adsorption at the surface, characterized by short-range attractions, plays a significant role in the adsorption of small proteins and can be mitigated by increasing the grafting density. Conversely, secondary adsorption, driven by van der Waals attraction, takes place at the outer periphery of the brush. On the other hand, there is still a lack of a universal theory that can explain or predict adsorption isotherms on polymer brushes for all cases. The most likely sources of this variation include (i) adsorption processes that are kinetically controlled, (ii) long-range interactions between the protein and polymer brushes, and (iii) nonuniform grafting of the polymers onto the surfaces.

4. MACHINE-LEARNING DESIGN OF POLYMER BRUSHES

A wide array of polymer brushes, along with their associated functions and surface-grafting strategies, have been extensively documented for various fundamental studies and practical applications. Nevertheless, current experimental designs and computational simulations of polymer brushes still bear an empirical essence due to the intricate nature of polymers and their correlated structures and properties. Recent advancements in data-driven machine-learning approaches have expanded their scope beyond traditional research domains from drug discovery, image recognition, disease diagnosis, and transportation analysis to materials informatics, particularly for inorganic or solid materials[106] (e.g., metals,[107,108] ceramics,[109,110] zeolites,[111,112] metal−organic frameworks,[113,114] nanoparticles,[115,116] and semiconductors[117,118]), enabling the evaluation and prediction of specific properties (electronic/ionic conductivity,[119,120] catalytic activity,[121,122] photoluminescence,[123,124] thermodynamics,[125,126] and mechanical properties[127,128]).

However, unlike inorganic or solid materials characterized by well-defined structures and reliable data sets, the application of machine learning to soft materials with desired functions and properties is still in its infancy. Challenges persist in utilizing machine learning to establish qualitative or quantitative rules for the rational assessment and design of functional soft materials, including polymers, elastomers, and hydrogels. More specifically, when it comes to polymer brushes, there is a striking lack of machine-learning studies, not even a mention of experimental validation of computationally designed polymer brushes. Several significant barriers contribute to this deficiency. First, there is a notable absence of publicly available polymer brush data sets, necessitating researchers to manually compile experimental results from the literature to establish polymer brush databases. Second, the intrinsic structural complexity and diversity of polymers, coupled with their diverse surface properties, exacerbate the problem of unreliable data compilation. This issue arises because even identical polymer brushes may yield inconsistent data due to variations in experimental conditions, chemical/material purity, and synthesis methodologies across different laboratories.

Until now, as an initial step, machine-learning approaches have been applied to self-assembled monolayers (SAMs), which represent the simplest form of polymer brushes. These machine-learning approaches have predominantly used the same data set of SAMs, originating from the Whitesides group,[129] to construct various quantitative structure−activity relationship (QSAR) models, including descriptor-based linear (MLREM) and nonlinear (BRANNGP and BRANNLP) models,[130] descriptor-based artificial neural network (ANN) models,[131] and functional group-based ANN models,[132] for quantitatively assessing protein adsorption on both pre-existing and newly designed SAMs. Recently, an antifouling polymer brush data set containing 28 polymer brushes with a wide variety of chemical structures was constructed by carefully removing any redundant and inconsistent data from existing literature studies.[133] This data set served as the foundation for the development of two distinct machine-learning methodologies: (i) the ANN model with gross-level, property-based descriptors for repurposing/discovering the existing polymer brushes with antifouling properties and (ii) the supporting

https://doi.org/10.1021/acs.langmuir.3c03253
Langmuir 2024, 40, 1487−1502

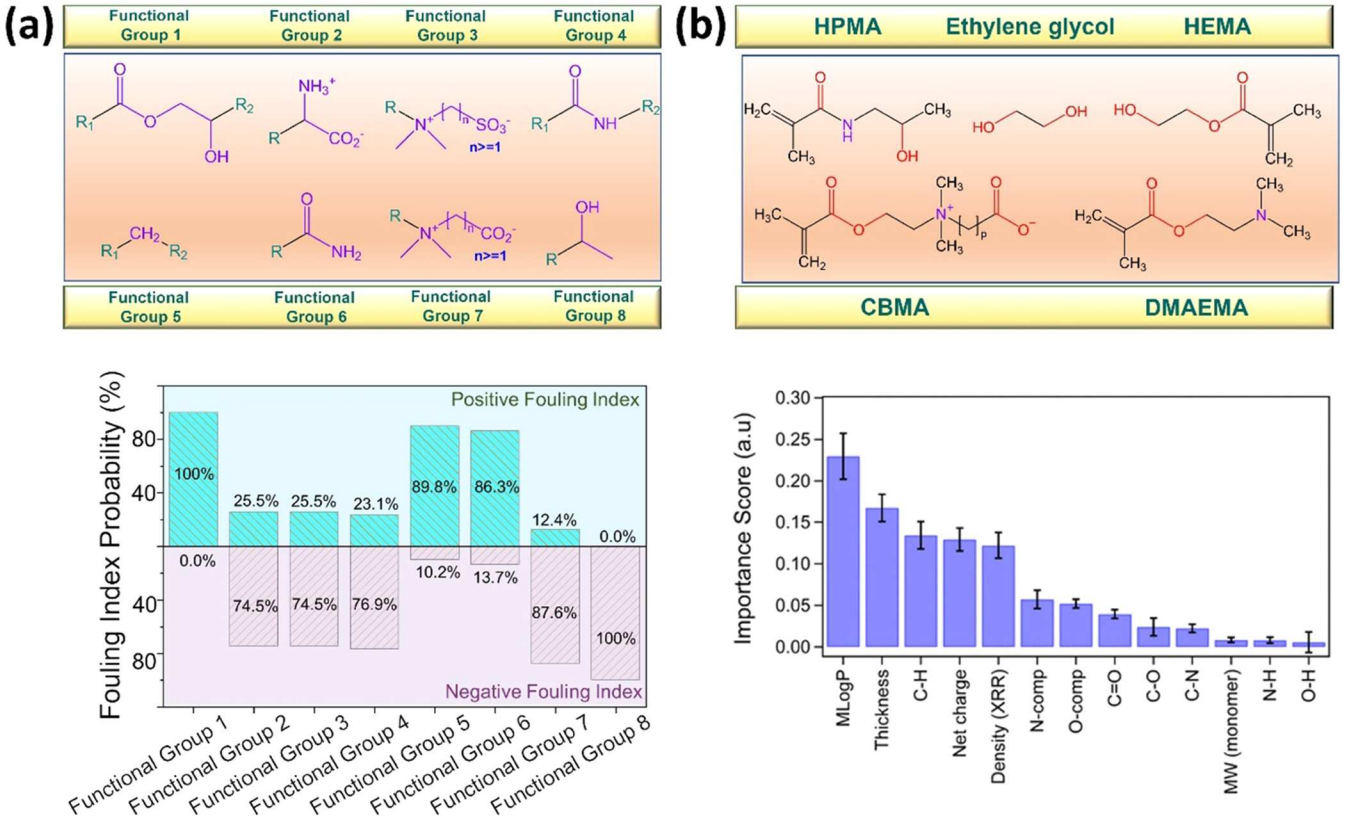

Figure 6. Machine-learning approaches for assessing the protein adsorption ability of existing and new antifouling polymer brushes. (a) Eight functional groups are identified and used to calculate their fouling index probability (%) in relation to protein adsorption on polymer brushes by a supporting vector regression (SVR) model. Reproduced with permission from refs 4,133. (b) Five monomers are used to determine the most relevant descriptors for their contributions to the predicted protein adsorption on polymer brush using a random forest (RF) regression model. Reproduced with permission from ref 134.

vector regression (SVR) model with fragmental-level, group-based descriptors for designing new antifouling polymer brushes (Figure 6a). Subsequently, both repurposed and newly designed polymer brushes were synthesized and applied as brush coatings, followed by the validation of their antifouling performance through surface plasma resonance (SPR) assays. SPR results demonstrated the exceptional surface resistance of the predicted polymer brushes to protein adsorption. This was substantiated by the minimal amount of adsorbed proteins, ranging from 0.0 to 9.0 ng/cm^2, which closely aligned with the model predictions. In 2022, another machine-learning study aimed to predict the amount of adsorbed serum protein on polymer brushes using a random forest (RF) regression algorithm.[134] To this end, they began with the creation of a uniform data set by synthesizing polymer brushes with varying thicknesses and molecular densities using five different monomers, followed by the characterization of both the monomers and the corresponding polymer brushes in terms of chemical structural parameters (atomic composition and chemical bonds), theoretical hydrophobicity ($M \log P$), structural parameters (thickness and density), and the amounts of serum proteins adsorbed on polymer brushes (Figure 6b). Among this set of descriptors, the RF algorithm identified critical parameters influencing protein adsorption amounts in the following order of importance: $M \log P$ > thickness and density of polymer brushes, the number of C−H bonds, the net charge of monomer, and the density of polymer brushes > N-comp, O-comp, C−O, C═O, C−N, MW, N−H, and O−H > monomer molecular weight, and the number of O−H bonds.

As pioneering studies, both of these machine-learning investigations on polymer brushes present a viable workflow. This process begins with the construction of data sets containing small but robust polymer brushes and extends to the development of machine-learning models. These models are used for both repurposing existing polymer brushes and designing new ones through an extensive screening of the spatial, compositional, and interaction spaces of polymers. As the field of polymer brushes continues to evolve, the availability of computationally designed and experimentally validated data holds the promise of further enhancing the iterative nature of machine learning in material design. With the advent of an extensive data set encompassing a wide range of polymers, brush structures, specific functions, and desirable properties, this iterative process not only accelerates material design but also enables the exploration of novel and previously uncharted territories in the polymer brush universe. The synergistic relationship between data-driven machine learning and the accumulation of empirical data will undoubtedly revolutionize the way we conceive, design, and engineer polymer brushes with unprecedented precision and efficiency to meet the demands of various industrial and scientific applications.

https://doi.org/10.1021/acs.langmuir.3c03253
Langmuir 2024, 40, 1487−1502

5. CONCLUSIONS

After years of extensive demonstrations, polymer brushes have emerged as a widely acknowledged and remarkably versatile toolbox, which facilitates the introduction of a diverse array of topological and functional versatility to virtually any substrate, spanning inorganics, organics, metals, semiconductors, and polymers. This versatility is achieved through nearly precise molecular control over surface-grafting density, thickness, roughness, polymer composition, conformation, and flexibility. Furthermore, most polymer synthesis methods, such as ATRP, RAFT, ROMP, and living anionic/cationic polymerization, can be readily adapted for the production of polymer brushes, thus enhancing their uses for different purposes. In light of mounting concerns and an increasing sense of urgency regarding health, energy, and environmental challenges, there is a compelling opportunity to integrate polymer brushes with nanoparticles, porous materials, and biomolecules, which offer the potential to unlock new functionalities in emerging fields and applications beyond their renowned antifouling characteristics. Considering the inherently nanoscale nature of polymer brushes, another crucial aspect is the development of macromanufacturing technologies aimed at upscaling the production of polymer brushes for some applications (e.g., smart devices) where large-area coatings or bulk materials are needed.

From a computational perspective, given the recent rapid advancements in data-driven artificial intelligence (AI), it remains a prudent strategy to explore the development of innovative data-/model-driven deep-learning algorithms, which help to expedite the rational design of new polymer brushes or the repurposing of existing ones. The initial and indispensable step in developing AI models for polymer brushes is the meticulous collection of reliable data sets from the literature to construct benchmark databases, although some advanced AI models have demonstrated their ability to extract essential structure−property relationships from relatively small compound data sets. It has proved to be a formidable challenge to construct a database from heterogeneous data sets obtained from different laboratories and under different experimental conditions. To address this challenge, it is essential to implement robust data quality control measures that encompass several strategies. One crucial strategy involves normalizing variables to ensure that data from multiple sources can be seamlessly compared and effectively utilized together. Furthermore, since these data sets often contain imperfections, such as missing values, biased outliers, or noisy data, data cleaning and preprocessing are essential and required. Second, once the database construction of polymer brushes is successfully accomplished, further research should be conducted to establish correlations between the chemical and structural characteristics of the polymer brush and their specific target functions. These target functions could encompass critical parameters such as determining protein adsorption amounts for antifouling polymer brushes, assessing membrane filtration performance for polymer brushes designed for membrane separation, evaluating electronic conductivity for conducting polymer brushes, or gauging biomolecular binding affinity for biosensor-based polymer brushes. The pursuit of such research in this direction is pivotal for achieving the optimal design of polymer brushes tailored to niche applications. Furthermore, both successful and unsuccessful design attempts can provide invaluable feedback for refining AI models through iterative data training and optimization processes. This iterative approach ultimately paves the way for highly efficient polymer brush designs. As a result, an AI-driven design strategy could furnish valuable structural templates for generating new polymer brush building blocks, significantly expanding a pool of polymer brushes.

In parallel to AI modeling, molecular simulations, including quantum mechanics, molecular dynamics, and Monte Carlo simulations, are still powerful tools to investigate the structure, dynamics, and interfacial properties of polymer brushes at atomic or coarse-grained resolution. However, employing molecular simulations to investigate polymer brushes is a multifaceted endeavor that involves numerous challenges. First, developing accurate force fields capable of capturing the conformational behavior of polymer brushes is an arduous and time-intensive task, necessitating robust validation against extensive experimental results. The intricacies of force field development can be particularly pronounced when dealing with diverse polymer brush systems. Particularly, transferable CG force fields across various polymer brush systems remain a state-of-the-art challenge. This is because different simulation systems may demand varying CG resolutions, specific potential energy functions, and even biased sampling techniques to achieve accurate results. Second, when tackling large polymer brush systems, choices pertaining to implicit solvent models, explicit solvent molecules, and polymer coarse-grained models play a pivotal role in the level of detail regarding solvent−polymer interactions and polymer−polymer interactions within simulations. These choices greatly influence the accuracy of the obtained results. Furthermore, in some systems involving highly charged or reactive species, quantum mechanical effects might be significant.[135] Incorporating these effects through methods such as quantum mechanics/molecular mechanics (QM/MM) simulations introduces an additional layer of complexity. Third, current simulations of polymer brushes typically involve constructing preformed polymer chains to create specific brush structures on a substrate at their lowest energy states. However, this approach can lead to the introduction of structural and packing artifacts. There is a notable absence of innovative algorithms designed to replicate the radical polymerization process, particularly grafting-from methods, which allow for the gradual growth of polymer chains directly from the substrate at atomic resolution. This omission is due to the inherent complexity of polymer architectures, polydispersity, and grafting density, which cannot be accurately represented by any available force fields. Looking ahead, advancements in hardware techniques, such as graphic processing units (GPU)-based simulations, coupled with sophisticated algorithms like kinetic theory, have the potential to enable a more comprehensive exploration of the intricate energy landscape associated with polymer brushes.

■ ASSOCIATED CONTENT

Special Issue Paper

Published as part of *Langmuir* virtual special issue "Highlights in Interface Science and Engineering: Polymer Brushes".

■ AUTHOR INFORMATION

Corresponding Author

Jie Zheng − *Department of Chemical, Biomolecular, and Corrosion Engineering, The University of Akron, Akron, Ohio 44325, United States;* orcid.org/0000-0003-1547-3612; Email: zhengj@uakron.edu

https://doi.org/10.1021/acs.langmuir.3c03253
Langmuir 2024, 40, 1487−1502

Authors

Yijing Tang − *Department of Chemical, Biomolecular, and Corrosion Engineering, The University of Akron, Akron, Ohio 44325, United States*

Yonglan Liu − *Department of Chemical, Biomolecular, and Corrosion Engineering, The University of Akron, Akron, Ohio 44325, United States*

Dong Zhang − *The Wallace H. Coulter Department of Biomedical Engineering at Georgia Tech and Emory University, Georgia Institute of Technology, Atlanta, Georgia 30332, United States;* orcid.org/0000-0001-7002-7661

Complete contact information is available at: https://pubs.acs.org/10.1021/acs.langmuir.3c03253

Notes

The authors declare no competing financial interest.

■ ACKNOWLEDGMENTS

The authors acknowledge financial support from the NSF Grant (DMR-2311985) and the ACS PRF Grant (ND-65277).

■ REFERENCES

(1) Barbey, R.; Lavanant, L.; Paripovic, D.; Schüwer, N.; Sugnaux, C.; Tugulu, S.; Klok, H.-A. Polymer brushes via surface-initiated controlled radical polymerization: synthesis, characterization, properties, and applications. *Chem. Rev.* **2009**, *109* (11), 5437−5527.

(2) Lee, H.-i.; Pietrasik, J.; Sheiko, S. S.; Matyjaszewski, K. Stimuli-responsive molecular brushes. *Prog. Polym. Sci.* **2010**, *35* (1), 24−44.

(3) Azzaroni, O. Polymer brushes here, there, and everywhere: Recent advances in their practical applications and emerging opportunities in multiple research fields. *J. Polym. Sci., Part A: Polym. Chem.* **2012**, *50* (16), 3225−3258.

(4) Li, Q.; Wen, C.; Yang, J.; Zhou, X.; Zhu, Y.; Zheng, J.; Cheng, G.; Bai, J.; Xu, T.; Ji, J.; Jiang, S.; Zhang, L.; Zhang, P. Zwitterionic Biomaterials. *Chem. Rev.* **2022**, *122* (23), 17073−17154.

(5) Zdyrko, B.; Luzinov, I. Polymer Brushes by the "Grafting to" Method. *Macromol. Rapid Commun.* **2011**, *32* (12), 859−869.

(6) Minko, S.; Patil, S.; Datsyuk, V.; Simon, F.; Eichhorn, K.-J.; Motornov, M.; Usov, D.; Tokarev, I.; Stamm, M. Synthesis of Adaptive Polymer Brushes via "Grafting To" Approach from Melt. *Langmuir* **2002**, *18* (1), 289−296.

(7) Pyun, J.; Kowalewski, T.; Matyjaszewski, K. Synthesis of Polymer Brushes Using Atom Transfer Radical Polymerization. *Macromol. Rapid Commun.* **2003**, *24* (18), 1043−1059.

(8) Edmondson, S.; Osborne, V. L.; Huck, W. T. S. Polymer brushes via surface-initiated polymerizations. *Chem. Soc. Rev.* **2004**, *33* (1), 14−22.

(9) van Eck, G. C. R.; Chiappisi, L.; de Beer, S. Fundamentals and Applications of Polymer Brushes in Air. *ACS Appl. Polym. Mater.* **2022**, *4* (5), 3062−3087.

(10) Krishnamoorthy, M.; Hakobyan, S.; Ramstedt, M.; Gautrot, J. E. Surface-initiated polymer brushes in the biomedical field: applications in membrane science, biosensing, cell culture, regenerative medicine and antibacterial coatings. *Chem. Rev.* **2014**, *114* (21), 10976−11026.

(11) Keating, J. J. I. V.; Imbrogno, J.; Belfort, G. Polymer Brushes for Membrane Separations: A Review. *ACS Appl. Mater. Interfaces* **2016**, *8* (42), 28383−28399.

(12) Lichter, J. A.; Van Vliet, K. J.; Rubner, M. F. Design of Antibacterial Surfaces and Interfaces: Polyelectrolyte Multilayers as a Multifunctional Platform. *Macromolecules* **2009**, *42* (22), 8573−8586.

(13) Zhao, C.; Li, L.; Zheng, J. Achieving highly effective nonfouling performance for surface-grafted poly(HPMA) via atom-transfer radical polymerization. *Langmuir* **2010**, *26* (22), 17375−17382.

(14) Chen, H.; Zhao, C.; Zhang, M.; Chen, Q.; Ma, J.; Zheng, J. Molecular understanding and structural-based design of polyacrylamides and polyacrylates as antifouling materials. *Langmuir* **2016**, *32* (14), 3315−3330.

(15) Gunkel, G.; Weinhart, M.; Becherer, T.; Haag, R.; Huck, W. T. S. Effect of polymer brush architecture on antibiofouling properties. *Biomacromolecules* **2011**, *12* (11), 4169−4172.

(16) Liu, J.; Zheng, N.; Li, Z.; Liu, Z.; Wang, G.; Gui, L.; Lin, J. Fast self-healing and antifouling polyurethane/fluorinated polysiloxane-microcapsules-silica composite material. *Adv. Compos. Hybrid Mater.* **2022**, *5* (3), 1899−1909.

(17) Marx, K. A. Quartz Crystal Microbalance: A Useful Tool for Studying Thin Polymer Films and Complex Biomolecular Systems at the Solution−Surface Interface. *Biomacromolecules* **2003**, *4* (5), 1099−1120.

(18) Lutolf, M. P.; Hubbell, J. A. Synthetic biomaterials as instructive extracellular microenvironments for morphogenesis in tissue engineering. *Nat. Biotechnol.* **2005**, *23* (1), 47−55.

(19) Wilson, C. J.; Clegg, R. E.; Leavesley, D. I.; Pearcy, M. J. Mediation of Biomaterial−Cell Interactions by Adsorbed Proteins: A Review. *Tissue Eng.* **2005**, *11* (1−2), 1−18.

(20) Jeon, N. L.; Choi, I. S.; Whitesides, G. M.; Kim, N. Y.; Laibinis, P. E.; Harada, Y.; Finnie, K. R.; Girolami, G. S.; Nuzzo, R. G. Patterned polymer growth on silicon surfaces using microcontact printing and surface-initiated polymerization. *Appl. Phys. Lett.* **1999**, *75* (26), 4201−4203.

(21) Husseman, M.; Malmström, E. E.; McNamara, M.; Mate, M.; Mecerreyes, D.; Benoit, D. G.; Hedrick, J. L.; Mansky, P.; Huang, E.; Russell, T. P.; Hawker, C. J. Controlled Synthesis of Polymer Brushes by "Living" Free Radical Polymerization Techniques. *Macromolecules* **1999**, *32* (5), 1424−1431.

(22) Wang, J.-S.; Matyjaszewski, K. Controlled/"living" radical polymerization. atom transfer radical polymerization in the presence of transition-metal complexes. *J. Am. Chem. Soc.* **1995**, *117* (20), 5614−5615.

(23) Ding, S.; Floyd, J. A.; Walters, K. B. Comparison of surface confined ATRP and SET-LRP syntheses for a series of amino (meth)acrylate polymer brushes on silicon substrates. *J. Polym. Sci., Part A: Polym. Chem.* **2009**, *47* (23), 6552−6560.

(24) Baum, M.; Brittain, W. J. Synthesis of Polymer Brushes on Silicate Substrates via Reversible Addition Fragmentation Chain Transfer Technique. *Macromolecules* **2002**, *35* (3), 610−615.

(25) Luzinov, I.; Minko, S.; Tsukruk, V. V. Responsive brush layers: from tailored gradients to reversibly assembled nanoparticles. *Soft Matter* **2008**, *4* (4), 714−725.

(26) van der Waarden, M. Stabilization of carbon-black dispersions in hydrocarbons. *J. Colloid Sci.* **1950**, *5* (4), 317−325.

(27) Mackor, E. L.; van der Waals, J. H. The statistics of the adsorption of rod-shaped molecules in connection with the stability of certain colloidal dispersions. *J. Colloid Sci.* **1952**, *7* (5), 535−550.

(28) Willner, I. Biomaterials for Sensors, Fuel Cells, and Circuitry. *Science* **2002**, *298* (5602), 2407−2408.

(29) Zhang, Z. B.; Yuan, S. J.; Zhu, X. L.; Neoh, K. G.; Kang, E. T. Enzyme-mediated amperometric biosensors prepared via successive surface-initiated atom-transfer radical polymerization. *Biosens. Bioelectron.* **2010**, *25* (5), 1102−1108.

(30) Yu, Q.; Zhang, Y.; Chen, H.; Zhou, F.; Wu, Z.; Huang, H.; Brash, J. L. Protein Adsorption and Cell Adhesion/Detachment Behavior on Dual-Responsive Silicon Surfaces Modified with Poly(N-isopropylacrylamide)-block-polystyrene Copolymer. *Langmuir* **2010**, *26* (11), 8582−8588.

(31) Jonas, A. M.; Glinel, K.; Oren, R.; Nysten, B.; Huck, W. T. S. Thermo-Responsive Polymer Brushes with Tunable Collapse Temperatures in the Physiological Range. *Macromolecules* **2007**, *40* (13), 4403−4405.

(32) Tugulu, S.; Silacci, P.; Stergiopulos, N.; Klok, H.-A. RGD—Functionalized polymer brushes as substrates for the integrin specific adhesion of human umbilical vein endothelial cells. *Biomaterials* **2007**, *28* (16), 2536−2546.

(33) Sato, T.; Morinaga, T.; Marukane, S.; Narutomi, T.; Igarashi, T.; Kawano, Y.; Ohno, K.; Fukuda, T.; Tsujii, Y. Novel Solid-State

Polymer Electrolyte of Colloidal Crystal Decorated with Ionic-Liquid Polymer Brush. *Adv. Mater.* **2011**, *23* (42), 4868−4872.
(34) Kim, B. Y.; Ratcliff, E. L.; Armstrong, N. R.; Kowalewski, T.; Pyun, J. Ferrocene Functional Polymer Brushes on Indium Tin Oxide via Surface-Initiated Atom Transfer Radical Polymerization. *Langmuir* **2010**, *26* (3), 2083−2092.
(35) Wang, Y.-H.; Hung, M.-K.; Lin, C.-H.; Lin, H.-C.; Lee, J.-T. Patterned nitroxide polymer brushes for thin-film cathodes in organic radical batteries. *Chem. Commun.* **2011**, *47* (4), 1249−1251.
(36) Komaba, S.; Ishikawa, T.; Yabuuchi, N.; Murata, W.; Ito, A.; Ohsawa, Y. Fluorinated Ethylene Carbonate as Electrolyte Additive for Rechargeable Na Batteries. *ACS Appl. Mater. Interfaces* **2011**, *3* (11), 4165−4168.
(37) Costantini, F.; Bula, W. P.; Salvio, R.; Huskens, J.; Gardeniers, H. J. G. E.; Reinhoudt, D. N.; Verboom, W. Nanostructure Based on Polymer Brushes for Efficient Heterogeneous Catalysis in Microreactors. *J. Am. Chem. Soc.* **2009**, *131* (5), 1650−1651.
(38) Costantini, F.; Benetti, E. M.; Tiggelaar, R. M.; Gardeniers, H. J. G. E.; Reinhoudt, D. N.; Huskens, J.; Vancso, G. J.; Verboom, W. A Brush-Gel/Metal-Nanoparticle Hybrid Film as an Efficient Supported Catalyst in Glass Microreactors. *Chem. − Eur. J.* **2010**, *16* (41), 12406−12411.
(39) Tokareva, I.; Minko, S.; Fendler, J. H.; Hutter, E. Nanosensors Based on Responsive Polymer Brushes and Gold Nanoparticle Enhanced Transmission Surface Plasmon Resonance Spectroscopy. *J. Am. Chem. Soc.* **2004**, *126* (49), 15950−15951.
(40) Mitsuishi, M.; Koishikawa, Y.; Tanaka, H.; Sato, E.; Mikayama, T.; Matsui, J.; Miyashita, T. Nanoscale Actuation of Thermoreversible Polymer Brushes Coupled with Localized Surface Plasmon Resonance of Gold Nanoparticles. *Langmuir* **2007**, *23* (14), 7472−7474.
(41) Gupta, S.; Agrawal, M.; Uhlmann, P.; Simon, F.; Stamm, M. Poly(N-isopropyl acrylamide)−Gold Nanoassemblies on Macroscopic Surfaces: Fabrication, Characterization, and Application. *Chem. Mater.* **2010**, *22* (2), 504−509.
(42) Alexander, S. Adsorption of chain molecules with a polar head a scaling description. *J. Phys.* **1977**, *38* (8), 983−987.
(43) de Gennes, P. G. Conformations of polymers attached to an interface. *Macromolecules* **1980**, *13* (5), 1069−1075.
(44) Brittain, W. J.; Minko, S. A structural definition of polymer brushes. *J. Polym. Sci., Part A: Polym. Chem.* **2007**, *45* (16), 3505−3512.
(45) Niu, Y.; Bu, X.; Zhang, X. Single Chain Mean-Field Theory Study on Responsive Behavior of Semiflexible Polymer Brush. *Materials* **2021**, *14* (4), 778.
(46) Halperin, A. Polymer Brushes that Resist Adsorption of Model Proteins: Design Parameters. *Langmuir* **1999**, *15* (7), 2525−2533.
(47) Dimitrov, D. I.; Milchev, A.; Binder, K. Polymer brushes in solvents of variable quality: Molecular dynamics simulations using explicit solvent. *J. Chem. Phys.* **2007**, *127* (8), No. 084905.
(48) Rossi, G.; Elliott, I. G.; Ala-Nissila, T.; Faller, R. Molecular Dynamics Study of a MARTINI Coarse-Grained Polystyrene Brush in Good Solvent: Structure and Dynamics. *Macromolecules* **2012**, *45* (1), 563−571.
(49) Singh, M. K.; Ilg, P.; Espinosa-Marzal, R. M.; Kröger, M.; Spencer, N. D. Polymer Brushes under Shear: Molecular Dynamics Simulations Compared to Experiments. *Langmuir* **2015**, *31* (16), 4798−4805.
(50) Lyu, H.; Xu, F.; Merlitz, H.; Wu, C.-X. Chain stiffness effect on the properties of topological polymer brushes and the penetration by free chains using MD simulation. *J. Phys. Commun.* **2018**, *2* (1), No. 015025.
(51) Wang, L.; Zhong, T.; Quan, X.; Zhou, J. Solvent-responsiveness of PS−PEO binary mixed polymer brushes: a coarse-grained molecular dynamics study. *Mol. Simul.* **2017**, *43* (13−16), 1322−1330.
(52) Menichetti, R.; Pelissetto, A.; Randisi, F. Thermodynamics of star polymer solutions: A coarse-grained study. *J. Chem. Phys.* **2017**, *146* (24), No. 244908.
(53) Nielsen, S. O.; Carlos, F. L.; Goundla, S.; Michael, L. K. Coarse grain models and the computer simulation of soft materials. *J. Phys.: Condens. Matter* **2004**, *16* (15), R481 DOI: 10.1088/0953-8984/16/15/R03.
(54) Spyriouni, T.; Tzoumanekas, C.; Theodorou, D.; Müller-Plathe, F.; Milano, G. Coarse-Grained and Reverse-Mapped United-Atom Simulations of Long-Chain Atactic Polystyrene Melts: Structure, Thermodynamic Properties, Chain Conformation, and Entanglements. *Macromolecules* **2007**, *40* (10), 3876−3885.
(55) Xia, W.; Song, J.; Jeong, C.; Hsu, D. D.; Phelan, F. R., Jr.; Douglas, J. F.; Keten, S. Energy-Renormalization for Achieving Temperature Transferable Coarse-Graining of Polymer Dynamics. *Macromolecules* **2017**, *50* (21), 8787−8796.
(56) Benková, Z.; Szefczyk, B.; D S Cordeiro, M. N. Molecular Dynamics Study of Hydrated Poly(ethylene oxide) Chains Grafted on Siloxane Surface. *Macromolecules* **2011**, *44* (9), 3639−3648.
(57) Dahal, U. R.; Wang, Z.; Dormidontova, E. E. Hydration and Mobility of Poly(ethylene oxide) Brushes. *Macromolecules* **2017**, *50* (17), 6722−6732.
(58) Rodríguez-Ropero, F.; van der Vegt, N. F. A. Ionic specific effects on the structure, mechanics and interfacial softness of a polyelectrolyte brush. *Faraday Discuss.* **2013**, *160* (0), 297−309.
(59) Rahimian-Koloor, S. M. R.; Shokrieh, M. M. Investigating the Effect of the Curing-induced Residual Stress on the Mechanical Behavior of Carbon Nanotube/Epoxy Nanocomposites by Molecular Dynamics Simulation. *Eng. Sci.* **2023**, *22*, 817.
(60) Heinz, H.; Lin, T.-J.; Kishore Mishra, R.; Emami, F. S. Thermodynamically Consistent Force Fields for the Assembly of Inorganic, Organic, and Biological Nanostructures: The INTERFACE Force Field. *Langmuir* **2013**, *29* (6), 1754−1765.
(61) Jeon, S. I.; Lee, J. H.; Andrade, J. D.; de Gennes, P. G. Protein−surface interactions in the presence of polyethylene oxide: I. Simplified theory. *J. Colloid Interface Sci.* **1991**, *142* (1), 149−158.
(62) Coluzza, I.; Hansen, J.-P. Transition from Highly to Fully Stretched Polymer Brushes in Good Solvent. *Phys. Rev. Lett.* **2008**, *100* (1), No. 016104.
(63) Milner, S. T.; Witten, T. A.; Cates, M. E. Theory of the grafted polymer brush. *Macromolecules* **1988**, *21* (8), 2610−2619.
(64) McPherson, T.; Kidane, A.; Szleifer, I.; Park, K. Prevention of Protein Adsorption by Tethered Poly(ethylene oxide) Layers: Experiments and Single-Chain Mean-Field Analysis. *Langmuir* **1998**, *14* (1), 176−186.
(65) Fang, F.; Szleifer, I. Controlled release of proteins from polymer-modified surfaces. *Proc. Natl. Acad. Sci. U.S.A.* **2006**, *103* (15), 5769−5774.
(66) Szleifer, I. Protein adsorption on surfaces with grafted polymers: a theoretical approach. *Biophys. J.* **1997**, *72* (2), 595−612.
(67) Senaratne, W.; Andruzzi, L.; Ober, C. K. Self-Assembled Monolayers and Polymer Brushes in Biotechnology: Current Applications and Future Perspectives. *Biomacromolecules* **2005**, *6* (5), 2427−2448.
(68) Zheng, J.; Li, L.; Chen, S.; Jiang, S. Molecular simulation study of water interactions with oligo (ethylene glycol)-terminated alkanethiol self-assembled monolayers. *Langmuir* **2004**, *20* (20), 8931−8938.
(69) Zheng, J.; Li, L.; Tsao, H.-K.; Sheng, Y.-J.; Chen, S.; Jiang, S. Strong repulsive forces between protein and oligo (ethylene glycol) self-assembled monolayers: a molecular simulation study. *Biophys. J.* **2005**, *89* (1), 158−166.
(70) Zheng, J.; He, Y.; Chen, S.; Li, L.; Bernards, M. T.; Jiang, S. Molecular simulation studies of the structure of phosphorylcholine self-assembled monolayers. *J. Chem. Phys.* **2006**, *125* (17), 174714−174717.
(71) Chen, S.; Zheng, J.; Li, L.; Jiang, S. Strong resistance of phosphorylcholine self-assembled monolayers to protein adsorption: insights into nonfouling properties of zwitterionic materials. *J. Am. Chem. Soc.* **2005**, *127* (41), 14473−14478.
(72) Choi, Y. K.; Park, S.-J.; Park, S.; Kim, S.; Kern, N. R.; Lee, J.; Im, W. CHARMM-GUI Polymer Builder for Modeling and

https://doi.org/10.1021/acs.langmuir.3c03253
Langmuir 2024, 40, 1487−1502

Simulation of Synthetic Polymers. *J. Chem. Theory Comput.* **2021**, *17* (4), 2431−2443.
(73) Lai, P. Y.; Binder, K. Structure and dynamics of grafted polymer layers: A Monte Carlo simulation. *J. Chem. Phys.* **1991**, *95* (12), 9288−9299.
(74) Lai, P. Y.; Binder, K. Structure and dynamics of polymer brushes near the Θ point: A Monte Carlo simulation. *J. Chem. Phys.* **1992**, *97* (1), 586−595.
(75) O'Shea, S. J.; Welland, M. E.; Rayment, T. An atomic force microscope study of grafted polymers on mica. *Langmuir* **1993**, *9* (7), 1826−1835.
(76) Zhao, W.; Krausch, G.; Rafailovich, M. H.; Sokolov, J. Lateral Structure of a Grafted Polymer Layer in a Poor Solvent. *Macromolecules* **1994**, *27* (11), 2933−2935.
(77) Wan, W.-B.; Lv, H.-H.; Merlitz, H.; Wu, C.-X. Static and dynamic properties of polymer brush with topological ring structures: Molecular dynamic simulation. *Chin. Phys. B* **2016**, *25* (10), No. 106101.
(78) Lee, H.; de Vries, A. H.; Marrink, S.-J.; Pastor, R. W. A Coarse-Grained Model for Polyethylene Oxide and Polyethylene Glycol: Conformation and Hydrodynamics. *J. Phys. Chem. B* **2009**, *113* (40), 13186−13194.
(79) Polanowski, P.; Hałagan, K.; Pietrasik, J.; Jeszka, J. K.; Matyjaszewski, K. Growth of polymer brushes by "grafting from" via ATRP − Monte Carlo simulations. *Polymer* **2017**, *130*, 267−279.
(80) Bedrov, D.; Smith, G. D. Molecular Dynamics Simulation Study of the Structure of Poly(ethylene oxide) Brushes on Nonpolar Surfaces in Aqueous Solution. *Langmuir* **2006**, *22* (14), 6189−6194.
(81) Roosjen, A.; van der Mei, H. C.; Busscher, H. J.; Norde, W. Microbial Adhesion to Poly(ethylene oxide) Brushes: Influence of Polymer Chain Length and Temperature. *Langmuir* **2004**, *20* (25), 10949−10955.
(82) Elliott, I. G.; Kuhl, T. L.; Faller, R. Molecular Simulation Study of the Structure of High Density Polymer Brushes in Good Solvent. *Macromolecules* **2010**, *43* (21), 9131−9138.
(83) Murakami, D.; Kobayashi, M.; Higaki, Y.; Jinnai, H.; Takahara, A. Swollen structure and electrostatic interactions of polyelectrolyte brush in aqueous solution. *Polymer* **2016**, *98*, 464−469.
(84) Santos, D. E. S.; Li, D.; Ramstedt, M.; Gautrot, J. E.; Soares, T. A. Conformational Dynamics and Responsiveness of Weak and Strong Polyelectrolyte Brushes: Atomistic Simulations of Poly-(dimethyl aminoethyl methacrylate) and Poly(2-(methacryloyloxy)-ethyl trimethylammonium chloride). *Langmuir* **2019**, *35* (14), 5037−5049.
(85) Stanzione, F.; Jayaraman, A. Computational Design of Oligopeptide Containing Poly(ethylene glycol) Brushes for Stimuli-Responsive Drug Delivery. *J. Phys. Chem. B* **2015**, *119* (42), 13309−13320.
(86) Galuschko, A.; Spirin, L.; Kreer, T.; Johner, A.; Pastorino, C.; Wittmer, J.; Baschnagel, J. Frictional Forces between Strongly Compressed, Nonentangled Polymer Brushes: Molecular Dynamics Simulations and Scaling Theory. *Langmuir* **2010**, *26* (9), 6418−6429.
(87) Goujon, F.; Malfreyt, P.; Tildesley, D. J. The compression of polymer brushes under shear: the friction coefficient as a function of compression, shear rate and the properties of the solvent. *Mol. Phys.* **2005**, *103* (19), 2675−2685.
(88) Kreer, T.; Müser, M. H.; Binder, K.; Klein, J. Frictional Drag Mechanisms between Polymer-Bearing Surfaces. *Langmuir* **2001**, *17* (25), 7804−7813.
(89) Irfachsyad, D.; Tildesley, D.; Malfreyt, P. Dissipative particle dynamics simulation of grafted polymer brushes under shear. *Phys. Chem. Chem. Phys.* **2002**, *4* (13), 3008−3015.
(90) Kreer, T.; Binder, K.; Müser, M. H. Friction between Polymer Brushes in Good Solvent Conditions: Steady-State Sliding versus Transient Behavior. *Langmuir* **2003**, *19* (18), 7551−7559.
(91) Zaloj, V.; Urbakh, M.; Klafter, J. Atomic Scale Friction: What can be Deduced from the Response to a Harmonic Drive? *Phys. Rev. Lett.* **1998**, *81* (6), 1227−1230.
(92) Kreer, T.; Müser, M. H. On the tribology and rheology of polymer brushes in good solvent conditions: a molecular dynamics study. *Wear* **2003**, *254* (9), 827−831.
(93) Chen, S.; Li, L.; Zhao, C.; Zheng, J. Surface hydration: Principles and applications toward low-fouling/nonfouling biomaterials. *Polymer* **2010**, *51* (23), 5283−5293.
(94) Li, L.; Chen, S.; Jiang, S. Protein interactions with oligo(ethylene glycol) (OEG) self-assembled monolayers: OEG stability, surface packing density and protein adsorption. *J. Biomater. Sci., Polym. Ed.* **2007**, *18*, 1415−1427.
(95) Vogler, E. A. Structure and reactivity of water at biomaterial surfaces. *Adv. Colloid Interface Sci.* **1998**, *74* (1), 69−117.
(96) Xiang, Y.; Xu, R.-G.; Leng, Y. Molecular Dynamics Simulations of a Poly(ethylene glycol)-Grafted Polyamide Membrane and Its Interaction with a Calcium Alginate Gel. *Langmuir* **2016**, *32* (18), 4424−4433.
(97) Liu, Z.-Y.; Jiang, Q.; Jin, Z.; Sun, Z.; Ma, W.; Wang, Y. Understanding the Antifouling Mechanism of Zwitterionic Monomer-Grafted Polyvinylidene Difluoride Membranes: A Comparative Experimental and Molecular Dynamics Simulation Study. *ACS Appl. Mater. Interfaces* **2019**, *11* (15), 14408−14417.
(98) Xiang, Y.; Xu, R.-G.; Leng, Y. Molecular Simulations of the Hydration Behavior of a Zwitterion Brush Array and Its Antifouling Property in an Aqueous Environment. *Langmuir* **2018**, *34* (6), 2245−2257.
(99) Xiang, Y.; Xu, R.-G.; Leng, Y. Molecular Understanding of Ion Effect on Polyzwitterion Conformation in an Aqueous Environment. *Langmuir* **2020**, *36* (26), 7648−7657.
(100) Shao, Q.; He, Y.; White, A. D.; Jiang, S. Difference in hydration between carboxybetaine and sulfobetaine. *J. Phys. Chem. B* **2010**, *114* (49), 16625−16631.
(101) Shao, Q.; He, Y.; Jiang, S. Molecular dynamics simulation study of ion interactions with zwitterions. *J. Phys. Chem. B* **2011**, *115* (25), 8358−8363.
(102) Cheung, D. L.; Lau, K. H. A. Atomistic Study of Zwitterionic Peptoid Antifouling Brushes. *Langmuir* **2019**, *35* (5), 1483−1494.
(103) Liu, Y.; Zhang, D.; Ren, B.; Gong, X.; Liu, A.; Chang, Y.; He, Y.; Zheng, J. Computational Investigation of Antifouling Property of Polyacrylamide Brushes. *Langmuir* **2020**, *36* (11), 2757−2766.
(104) Liu, Y.; Zhang, D.; Ren, B.; Gong, X.; Xu, L.; Feng, Z.-Q.; Chang, Y.; He, Y.; Zheng, J. Molecular simulations and understanding of antifouling zwitterionic polymer brushes. *J. Mater. Chem. B* **2020**, *8* (17), 3814−3828.
(105) Wyszogrodzka, M.; Haag, R. Synthesis and Characterization of Glycerol Dendrons, Self-Assembled Monolayers on Gold: A Detailed Study of Their Protein Resistance. *Biomacromolecules* **2009**, *10* (5), 1043−1054.
(106) Schmidt, J.; Marques, M. R. G.; Botti, S.; Marques, M. A. L. Recent advances and applications of machine learning in solid-state materials science. *npj Comput. Mater.* **2019**, *5* (1), 83.
(107) Zhao, H.; Ezeh, C. I.; Ren, W.; Li, W.; Pang, C. H.; Zheng, C.; Gao, X.; Wu, T. Integration of machine learning approaches for accelerated discovery of transition-metal dichalcogenides as Hg0 sensing materials. *Appl. Energy* **2019**, *254*, No. 113651.
(108) Fung, V.; Hu, G.; Ganesh, P.; Sumpter, B. G. Machine learned features from density of states for accurate adsorption energy prediction. *Nat. Commun.* **2021**, *12* (1), No. 88.
(109) Kaufmann, K.; Maryanovsky, D.; Mellor, W. M.; Zhu, C.; Rosengarten, A. S.; Harrington, T. J.; Oses, C.; Toher, C.; Curtarolo, S.; Vecchio, K. S. Discovery of high-entropy ceramics via machine learning. *npj Comput. Mater.* **2020**, *6* (1), 42.
(110) Balachandran, P. V.; Kowalski, B.; Sehirlioglu, A.; Lookman, T. Experimental search for high-temperature ferroelectric perovskites guided by two-step machine learning. *Nat. Commun.* **2018**, *9* (1), No. 1668.
(111) Moliner, M.; Román-Leshkov, Y.; Corma, A. Machine Learning Applied to Zeolite Synthesis: The Missing Link for Realizing High-Throughput Discovery. *Acc. Chem. Res.* **2019**, *52* (10), 2971−2980.

https://doi.org/10.1021/acs.langmuir.3c03253
Langmuir 2024, 40, 1487−1502

(112) Lin, S.; Wang, Y.; Zhao, Y.; Pericchi, L. R.; Hernández-Maldonado, A. J.; Chen, Z. Machine-learning-assisted screening of pure-silica zeolites for effective removal of linear siloxanes and derivatives. *J. Mater. Chem. A* **2020**, *8* (6), 3228−3237.
(113) Batra, R.; Chen, C.; Evans, T. G.; Walton, K. S.; Ramprasad, R. Prediction of water stability of metal−organic frameworks using machine learning. *Nat. Mach. Intell.* **2020**, *2* (11), 704−710.
(114) Moghadam, P. Z.; Rogge, S. M.; Li, A.; Chow, C.-M.; Wieme, J.; Moharrami, N.; Aragones-Anglada, M.; Conduit, G.; Gomez-Gualdron, D. A.; Van Speybroeck, V.; Fairen-Jimenez, D. Structure-mechanical stability relations of metal-organic frameworks via machine learning. *Matter* **2019**, *1* (1), 219−234.
(115) Yao, L.; Ou, Z.; Luo, B.; Xu, C.; Chen, Q. Machine learning to reveal nanoparticle dynamics from liquid-phase tem videos. *ACS Cent. Sci.* **2020**, *6* (8), 1421−1430.
(116) He, J.; He, C.; Zheng, C.; Wang, Q.; Ye, J. Plasmonic nanoparticle simulations and inverse design using machine learning. *Nanoscale* **2019**, *11* (37), 17444−17459.
(117) Tanaka, K.; Hachiya, K.; Zhang, W.; Matsuda, K.; Miyauchi, Y. Machine-Learning Analysis to Predict the Exciton Valley Polarization Landscape of 2D Semiconductors. *ACS Nano* **2019**, *13* (11), 12687−12693.
(118) Mannodi-Kanakkithodi, A.; Toriyama, M. Y.; Sen, F. G.; Davis, M. J.; Klie, R. F.; Chan, M. K. Machine-learned impurity level prediction for semiconductors: The example of Cd-based chalcogenides. *npj Comput. Mater.* **2020**, *6* (1), 39.
(119) Wu, S.; Kondo, Y.; Kakimoto, M.-a.; Yang, B.; Yamada, H.; Kuwajima, I.; Lambard, G.; Hongo, K.; Xu, Y.; Shiomi, J.; et al. Machine-learning-assisted discovery of polymers with high thermal conductivity using a molecular design algorithm. *npj Comput. Mater.* **2019**, *5* (1), 66.
(120) Mortazavi, B.; Podryabinkin, E. V.; Roche, S.; Rabczuk, T.; Zhuang, X.; Shapeev, A. V. Machine-learning interatomic potentials enable first-principles multiscale modeling of lattice thermal conductivity in graphene/borophene heterostructures. *Mater. Horiz.* **2020**, *7* (9), 2359−2367.
(121) Kitchin, J. R. Machine learning in catalysis. *Nat. Catal.* **2018**, *1* (4), 230−232.
(122) Yang, Z.; Gao, W.; Jiang, Q. A machine learning scheme for the catalytic activity of alloys with intrinsic descriptors. *J. Mater. Chem. A* **2020**, *8* (34), 17507−17515.
(123) Brown, K. A.; Brittman, S.; Maccaferri, N.; Jariwala, D.; Celano, U. Machine Learning in Nanoscience: Big Data at Small Scales. *Nano Lett.* **2020**, *20* (1), 2−10.
(124) Zhuo, Y.; Tehrani, A. M.; Oliynyk, A. O.; Duke, A. C.; Brgoch, J. Identifying an efficient, thermally robust inorganic phosphor host via machine learning. *Nat. Commun.* **2018**, *9* (1), No. 4377.
(125) Stanev, V.; Oses, C.; Kusne, A. G.; Rodriguez, E.; Paglione, J.; Curtarolo, S.; Takeuchi, I. Machine learning modeling of superconducting critical temperature. *npj Comput. Mater.* **2018**, *4* (1), 29.
(126) Wang, Q.; Ding, J.; Zhang, L.; Podryabinkin, E.; Shapeev, A.; Ma, E. Predicting the propensity for thermally activated β events in metallic glasses via interpretable machine learning. *npj Comput. Mater.* **2020**, *6* (1), 194.
(127) Wang, C.; Fu, H.; Jiang, L.; Xue, D.; Xie, J. A property-oriented design strategy for high performance copper alloys via machine learning. *npj Comput. Mater.* **2019**, *5* (1), 87.
(128) Hu, Y.-J.; Zhao, G.; Zhang, M.; Bin, B.; Del Rose, T.; Zhao, Q.; Zu, Q.; Chen, Y.; Sun, X.; de Jong, M.; Qi, L. Predicting densities and elastic moduli of SiO 2-based glasses by machine learning. *npj Comput. Mater.* **2020**, *6* (1), 25 DOI: 10.1038/s41524-020-0291-z.
(129) Ostuni, E.; Chapman, R. G.; Holmlin, R. E.; Takayama, S.; Whitesides, G. M. A survey of structure-property relationships of surfaces that resist the adsorption of protein. *Langmuir* **2001**, *17* (18), 5605−5620.
(130) Le, T. C.; Penna, M.; Winkler, D. A.; Yarovsky, I. Quantitative design rules for protein-resistant surface coatings using machine learning. *Sci. Rep.* **2019**, *9* (1), No. 265.
(131) Kwaria, R. J.; Mondarte, E. A. Q.; Tahara, H.; Chang, R.; Hayashi, T. Data-Driven Prediction of Protein Adsorption on Self-Assembled Monolayers toward Material Screening and Design. *ACS Biomater. Sci. Eng.* **2020**, *6* (9), 4949−4956.
(132) Liu, Y.; Zhang, D.; Tang, Y.; Zhang, Y.; Chang, Y.; Zheng, J. Machine Learning-Enabled Design and Prediction of Protein Resistance on Self-Assembled Monolayers and Beyond. *ACS Appl. Mater. Interfaces* **2021**, *13* (9), 11306−11319.
(133) Liu, Y.; Zhang, D.; Tang, Y.; Zhang, Y.; Gong, X.; Xie, S.; Zheng, J. Machine Learning-Enabled Repurposing and Design of Antifouling Polymer Brushes. *Chem. Eng. J.* **2021**, *420*, No. 129872.
(134) Palai, D.; Tahara, H.; Chikami, S.; Latag, G. V.; Maeda, S.; Komura, C.; Kurioka, H.; Hayashi, T. Prediction of Serum Adsorption onto Polymer Brush Films by Machine Learning. *ACS Biomater. Sci. Eng.* **2022**, *8* (9), 3765−3772.
(135) AlGemayel, C.; Zeaiter, J.; Talih, S.; Saliba, N. A.; Shihadeh, A. Mechanistic Analysis of the Pyrolysis of Vegetable Glycerin: A Reactive Force Field−Molecular Dynamics Study. *Eng. Sci.* **2023**, *23*, 885.

https://doi.org/10.1021/acs.langmuir.3c03253
Langmuir 2024, 40, 1487−1502